Experimental and Numerical investigation of flow structures behind Bluff Bodies in Tandem Arrangement

Golnaz Dianat

Submitted to the
Institute of Graduate Studies and Research
In partial fulfillment of the requirements for the Degree of

Master of Science
in
Mechanical Engineering

Eastern Mediterranean University
September 2011
Gazimağusa, North Cyprus

Approval of the Institute of Graduate Studies and Research

Prof. Dr. Elvan Yılmaz
Director

I certify that this thesis satisfies the requirements as a thesis for the degree of Master of Science in Mechanical Engineering.

Assoc. Prof. Dr. Ugur Atikol
Chair, Department of Mechanical Engineering

We certify that we have read this thesis and that in our opinion it is fully adequate in scope and quality as a thesis for the degree of Master of Science in Mechanical Engineering.

Asst. Prof. Dr. Hasan Hacışevki

Examining Committee

1. Prof. Dr. Majid Hashemipour

2. Assoc. Prof. Dr. Fuat Egelioğlu

3. Asst. Prof. Dr. Hasan Hacışevki

ABSTRACT

Flow structures attracted scientist since many decades. When a fluid flows around a bluff body or an object moves within a fluid at different Reynolds numbers different flow regimes can be observed. The flow properties plays great importance in analysis of different applications. These properties either calculated with numerical or experimental techniques. Experimental studies are time consuming and more expensive. Developments in computers enabled scientist to analyse and simulate almost all flow conditions easily. But always these results must be compared with experimental results to have more healty conclusions.

In this study flow properties such as instantaneous velocity, normalized velocity and incoherent flow structures analyzed numerically behind two normal flat plates in tandem arrangement at six different gap ratios. Reynolds Stress Model versus Two-Equation Shear Stress Transport $k-\omega$ model compared effectively for different gap ratios. Also results of double tandem plates and square cylinder were examined.

Computational Fluid Dynamics (CFD) codes ANSYS/FLUENT 13.0® was used to simulate the flow around the normal flat plates. The equations of shear stress transport $k-\omega$ model and Reynolds Stress Model (RSM) were considered as solution techniques. But since, the validity of any theoretical prediction can only be assessed in practice, the comparison was done between numerical data and achieved data from the experiments, for both cases based on literature. The experiments were done on an open type sub-sonic

wind tunnel at Reynolds number of 33000 with turbulence intensity around 0.5-0.8%. The effects of gap ratio on the flow characteristics were tested for tandem arrangements. Experimental errors, high cost equipment and spending too much time on testing, result in fulfilling the problem by CFD processes. These numerical methods compared with experimental results to justify the effects of different turbulence model.

Keywords: CFD, Vortex Shedding, Incoherent Products, Bluff bodies in tandem

ÖZ

Akış yapıları bilim insanlarının ilgisini onlarca yıldan beri çekmektedir. Bir akışkan herhangi bir cismin etrafından akarken veya herhangi bir cisim akışkan içerisinde hareket ederken Reynolds sayısına bağlı olarak akış tipi ve akış yapıları değişmektedir. Değişik uygulamalarda akış özellikleri büyük önem taşımaktadır. Bu akış özellikleri sayısal veya deneysel teknikler ile hesaplama bilmektedir. Deneysel çalışmalar daha pahalı ve zaman istemektedir. Bilgisayar alanındaki gelişmeler bilim insanlarınn her türlü akış sistemini kolayca analiz edip simülasyon yapmasına olanak tanımıştır. Fakat bu sayısal bulguların deneysel neticelerle karşılaştırılıp mukayese edilmesi gerekmektedir.

Bu çalışmada arka arkaya dizilmiş iki düz plakanın altı değişik aralık oranları için hız, normalize edilmiş hız, inkoherent özellikler ve stres özellikleri incelenmiştir. Reynolds stres modeli ile iki denklem kesme gerilmesi transport $k-\omega$ modeli incelenmiştir. Ayrıcaiki düz plaka ile karenesnelerda incelenmiştir.

Bilgisayar destekli akışkanlar dinamiği (CFD) kodları ANSYS/FLUENT 13.0 ® programları kullanılarak dik iki düz plakanın arkasındaki akış simüle edilmiştir. Kesme gerilmesi transport $k-\omega$ model ve Reynolds Stress modeli (RSM) denklemleri çözüm teknikleri olarak kullanılmıştır. Fakat sayısal çalışmalar ın netic elerin geçerliliği diğer deneysel neticeler ile birlik te değ erlen dirildiği için literature bu yönde taranmıştır.Kullanılan deneysel neticeler açık sesaltı Reynolds numarası 33000 ve

türbülans yoğunluğu 0.5-0.8% olan bir rüzgar tünelinde yapılmıştır. Açıklık oranının arka arkaya dizilmiş plakaları nakış karakteristiği üzerine olan etkileri test edilmiştir. Deneysel hatalar, yüksek ekipman maliyeti ve fazla zaman harcanması deneysel çalışmalar yerine bilgisayar destekli akışkanlar dinamiği (CFD) uygulamalarını populer hale getirmiştir. Değişik turbülans modelleme etkileri deneysel metodlar ile mukayese edilmiştir.

Anahtar kelimeler: Bilgisayarlı Akışkanlar Dinamiği, Vorteks oluşumu, Koherent olmayan yapılar, Tandem dizilmiş geometrik yapılar.

ACKNOWLEDGMENT

It would have been impossible for me to complete this work without the help of the people who have supported me financially, emotionally and morally. First, I would want to acknowledge my supervisor, Asst. Prof. Dr. Hasan Hacışevki for his relentless efforts and supports in making this work a reality. The Department Chair Assoc. Prof. Dr. Ugur Atikol and all the lecturers of the department, but not limiting them only, have also in one way or the other given me selfless support. To them, I will always remain thankful. To crown it all, I would want to show my gratitude to my primary mentors who are my parents, and brothers for their endless support in everything I do in life. And the friends who helped me in this way. I will remain always indebted to you for everything.

TABLE OF CONTENTS

LIST OF FIGURES

NOMENCLATURE

$\mu =$ The first dynamic viscosity $[kg/m.s]$

$\lambda =$ The second coefficient of viscosity $[kg/m.s]$

$\beta =$ Coefficient of thermal expansion $[K]$

$\Phi =$ Dissipation function

$\rho =$ Density $[kg/m^3]$

$\varepsilon =$Dissipation rate $[m^2/s^3]$

$\omega =$Specific dissipation rate $[1/s]$

$u''^2 =$ Normal Reynolds Stress in $x-$direction $[m^2/s^2]$

$v''^2 =$ Normal Reynolds Stress in $y-$direction $[m^2/s^2]$

$C_D =$ Drag coefficient

$C_p =$ Specific heat at constant pressure $[J/kg.K]$

CFD= Computational Fluid Dynamics

$d =$ Width of the plate $[mm]$

$EFD =$ Experimental Fluid Dynamics

$EWT =$Enhanced Wall Treatment

g/d = Gap ratio

k = Kinetic energy $[m^2/s^2]$

LIF=Laser-Induced Fluorescence

$PISO$ = Pressure-Implicit with Splitting of Operators

Re = Reynolds number

RSM =Reynolds Stress Model

rms = Root Mean Square

$SST\ k-\omega$ =Shear Stress Transport Turbulence Model

St = Strouhal number

S_{Mx} = Total force on the element due to body forces in x directions $[N/m^2]$

S_{My} = Total force on the element due to body forces in y directions $[N/m^2]$

S_{Mz} = Total force on the element due to body forces in z directions $[N/m^2]$

T = Temperature $[K]$

u = Velocity in x direction $[m/s]$

v = Velocity in y direction $[m/s]$

w = Velocity in z direction $[m/s]$

Chapter 1

INTRODUCTION

1.1 Experimental Fluid Mechanics versus Computational Fluid Mechanics

Fluid mechanics problems which are associated with the flow behavior, at rest or in motion or in relation with solids, were analyzed historically by performing experimental investigations in wind tunnels. Experimental measurement results together with the observations of fluid behavior caused the advent of fluid flows' governing equations. These mathematical statements are the expressions of the conservations laws of mass, momentum and energy of fluid particles. Wind tunnel experiments engaged with inability to simulate the flow over large size bodies, such as ships and airplanes, or in other word tests deal with scale effects problems, together with the difficulties to model the environmental effects on test models. On the other hand the experimental investigation involves high cost experiments. These facts motivate engineers to think about more rapid and cheaper ways to analyze the fluid manner. These reasons together with the presence of mathematical physical formulations and the advent of digital computers result in utilization of computational fluid dynamics (CFD) in simulation of fluids engineering systems. Despite of the all great progress of CFD technology in the last 40 years in the aerospace branch, there are still too many problems that are simple in geometry but difficult to simulate even after too many simulations. Numerical solutions

can be obtained easily by the aid of this new technology. But the presences of many physical problems that still remain unresolved make the reliability of these solutions to stand on the fragile base. However, CFD is a powerful instrument, that has developed itself to a desired level of applicability, but it is not a magic tool to analyze any difficulties. The mentioned problems make CFD incapable to overwhelm the wind tunnel experiments at the present time but these two methods work parallel, since the validity of numerical predictions can only be assessed as they compare with the experimental results. CFD limitations come from the speed and memory of the computers, but developments of computers show that these restrictions are decreasing rapidly. According to the CFD advantages such as the ability of performing investigations on the flows that are experimentally difficult to control and capability to analysis the flows that are engaged with the need to design new prototypes which consume time while CFD requires no real physical model, and the mobility facility of CFD with its rapid responses together with unlimited number of details achieved from each run, make use of capability of this new technology as an essential part of any research. There are numbers of articles showing the comparisons between the CFD results with experimental results and many workshops that exist to discuss on the verification and validation of CFD which show the importance of developments in CFD and strong requirement for CFD as a practical analysis and design tool [1].

1.2 Statement of the Problem

The present study was performed numerically to check the verification and validation of CFD analysis in comparison with the available experiments in the literature (Appendix A). The CFD analysis of the present dissertation carried out on the unsteady circulating

fluid chunks passed from long cylinders, called vortices that have attracted attention for more than four decades. This thesis has investigated the flow properties such as Reynolds stresses or incoherent structures of the wake of flow past from two normal in-line flat plates at Reynolds 33000. The effects of, spacing ratio between the flat plates and selection of different turbulence modeling methods on the results were analyzed. To make these studies valuable CFD results were compared with the experimental one that was performed in the wind tunnel, to verify the different turbulence models effects. To make the CFD analysis compatible with the results of experiment, the geometry of CFD model designed to have the same shape as the wind tunnel to achieve the geometric similarity and the initial velocity of the experiment at any point applied on the CFD initialization process to have the kinematic similarity. ANSYS/FLUENT 13.0® was used for processing the solution.

1.3 Practical Significance of Vortex Shedding

The presence of the vortices near the body cause the generation of vibrations on the body, which may lead the body to resonate to dangerous levels if the vortices frequency be close or exceed the natural frequency of the body. For instance, Tacoma Narrows Bridge (1940) was failed because of the presence of the excessive vibration induced by vortex shedding [2]. Cross flow past from bluff bodies is present in many applications of engineering such as civil engineering, for instance critical instability in concrete cooling towers caused by vortex shedding may cause the towers to collapse. Mechanical engineering such as the case of heat exchangers and tubes is another engineering area that deals with the complex cross flow. Consequently, engineers must consider the effects of vortex shedding while designing equipment and structures that may subjected

to the high velocity flow or steady high winds. These practical significances caused the existence of too many articles in this area of aerodynamics.

1.4 Methodology

Numerical investigation performed to determine the flow characteristics behind two bluff bodies by CFD. The Gambit 2.2.30 ® program together with ANSYS/FLUENT 13.0 ® and Tecplot 360 2010 ® were used to simulate the flow. The flow considered as incompressible, unsteady flow. The shear stress transport (SST) $k-\omega$ model together with Reynolds stress model (RSM) were considered as viscous models.

In general, all problems in CFD follow these steps:

- Geometry- geometry is selected and geometry parameters are defined
- Grid generation- consist of both structured and unstructured grids
- Physics- flow properties, viscous model, compressible or incompressible conditions are determined
- Initial conditions and boundary conditions are applied
- Solve- spatial discretization scheme and numerical schemes considered together with required accuracy for the problem
- Processing- the program is running
- Results- the CFD results can be visualized at this part.

1.5 Discussion of the Chapters

The background information on the investigations done on the comparison between the CFD and experimental fluid dynamics are presented in literature survey in chapter 2.

The methods applied to collect the data and the reasons of how these methods were taken are introduced in the chapter 3 with the methodology title. In chapter four the interpretation on findings and comparison between the experimental and numerical result are illustrated by the aid of contours and graphs. And finally the conclusion of this study together with the recommendation for the future work is presented in chapter 5.

Chapter 2

LITERATURE REVIEW

2.1 Introduction

Analyzing the fluid flow behavior can be done by the aid of experimental and empirical studies. Many efforts have been done in order to study and investigate the characteristics of the fluid flows. These attempts result in new field of science which is called the 'Fluid Mechanics'. In other word, fluid mechanics is the consequence of the experimental studies and observations. The outcome of different tests, the widely usage of differential equations and mathematical relations caused obtaining the theoretical-applicable and up to date equations. As a result, there are two general methods to examine the fluid manner: 1) experimental method and 2) Theoretical or numerical method.

The analytical solutions that were obtained from the experimental observations were difficult to compute; therefore experiments remained the only suitable way to compute the flow properties in the past. As the time passes, the experimental equipments improved to give the more accurate and better results. Despite of all efforts in the developments of experimental apparatus, some experimental restrictions remained the same. Scale effects, environmental effects and high cost experiments made engineers to think about the cheaper methods that are capable to solve the scale effect problems.

Development and progress of computer science and programming brought about the genesis of Computational Fluid Dynamics (CFD) with the purpose of solving the numerical equations in the recent century. According to Professor Dean Chapman at Stanford University providing an important new technology capability and economics are two major motivations behind CFD and they will not change in the coming decades [3]. The large number of investigations on the validation and verification of CFD, as a practical analysis and design tool, are the proofs for the strong need for CFD.

Aerospace is one of the areas of CFD applications in the last 30 years. Some problems in this field still remain unknown, even with simple geometries and after many simulations. One of the fluid flow difficulties is the case of vortex shedding from bluff bodies that has attracted markedly attention for over four decades. The vortex shedding phenomenon is a consequence of flow movement over long cylinders and spheres as the Reynolds is greater than 90 [4]. The significance of these periodic unsteady flows past from bluff bodies comes from the wide range of their applications in engineering, such as offshore platforms and high tower buildings in civil engineering and tube and heat exchangers in mechanical engineering branch. In the layouts of these constructions multiple bluff bodies are available which make the flow complex [5]. Vortices are capable to produce the vibrations near the body which may result in the resonation of body to dangerous level if the frequencies of the vortices get close to the natural frequency of the body [4]. Interpreting the aerodynamics of buildings can assist practical engineers to design and build the safe and economical structures.

2.2 Experimental Investigations and Apparatus

In this section the focus is mainly on, the previous researches on the flow passed from the bluff bodies in different arrangements and the wake of these bodies. The presence of the different flow regimes and the variation in other flow variables are discussed as the distance between the bodies and the geometry of these bodies changed. The presented researches in this part are all done by experiments.

P.W. Bearman [6] performed experiments on two dimensional bluff bodies in a closed-return wind-tunnel at different Reynolds number between 1.4×10^5 and2.56×10^5. Traverses of the wake together with the base pressure and vortex shedding frequency were measured by using a hot wire anemometer. He found out that the peak in root-mean-square (rms) velocity fluctuation occurred at the position of the fully formed vortex. The research continued by fitting the splitter plates (up to four heights long) behind the rear face of the model. He discovered that the distance from the base model to the fully formed vortex is inversely proportional to the base pressure coefficient. Presence of the splitter plates cause reduction in the drag of a bluff body and in some cases suppress vortex formation as it has been known for a long time.

P. W.Bearman and D. M.Trueman [7] did some experimental investigations on two-dimensional rectangular plate, located perpendicular to the wind direction, in two closed-return wind tunnel with low turbulence level, but with different cross section areas. Despite of the well-known fact that, the drag coefficient of both thin flat plate and thicker body normal to wind direction in about 2.0, they could get the coefficient as high as 2.94. For this purpose, they started increasing the thickness of the two dimensional

rectangular plate from 0.2 to 1.2. The critical block dimension, where the maximum value of drag coefficient achieved, was when the thickness was just over the half of the width ($\frac{Thickness}{Width}$= 0.62).

According to P. W.Bearman and D. M. Trueman, high drag is a result of regular vortex shedding. Hot wire and a wave analyzer were used to detect and measure vortex shedding and frequency of shedding, respectively. Water tunnel was also applied for the flow visualization purposes. Bearman [8] has shown that the higher base pressure is a result of the formation of vortices away from the body. The distance to vortex formation and the strength of fully formed vortices are related to the amount of vorticity that is being shed from the body, which is determined by base pressure. The results of these experiments were in a good agreement with the findings in Japan.

Chi_Hung Liu and Jerry M.Chen [9] carried out different experiments, on two square cylinders in tandem arrangement, to investigate the effects of 1) ratio of the spacing between the square cylinders to the width of the cylinder, and 2) the manner of varying this spacing ratio, on the flow properties. The experiments were done in a low speed, open circuit wind tunnel. Spacing between the cylinders was changed in the way of progressive increase and progressive decrease, between the ranges from 1.5 to 9.0 widths. Reynolds numbers were also varied in the ranges of $2.0 \times 10^3 - 1.6 \times 10^4$. The hysteresis regime on drag observed for all Reynolds number, as drag forces that were obtained by integrating the mean pressure distributions for both upstream and downstream cylinders, as the spacing between the cylinders varied in a progressively increasing and decreasing manner. Two different flow patterns referred to mode I and

mode II where associated with two discontinues jumps that occurred in hysteresis regime, were observed. For both upstream and downstream cylinder, two branches of drag coefficient (C_D) were observed in the hysteresis regime. The progressive increase in the spacing is associated with the flow pattern called mode I and is referred to the lower branch. And the flow pattern of mode II is associated with the upper branch which is a result of progressive decrease in the spacing. They pointed out that there is only one stable mode occurs in the hysteresis regime despite of the, presence of the intermittent change between Mode I and Mode II for higher Reynolds numbers as mentioned by previous authors. They also showed that the flow characteristics depend strongly on the manner of the varying the spacing between the cylinders in addition to the well-known fact of their dependency to the spacing ratio. The presence of discontinuous jump in each flow pattern is associated with hysteresis. For the low Reynolds number, the values of upper and lower spacing limits of the hysteresis regime are large. As the Reynolds number increased to 300 and beyond, the spacing limits leveled off rapidly. Further increase in the Reynolds number result in having the spacing limits at a nearly constant value of $1.0D$ independent from Reynolds number. Both drag coefficient and fluctuating pressure of two cylinders for Mode I are in lower level than the computed values for Mode II. Chain_Hung Liu and Jerry M.Chen demonstrated the changes in Strouhal Number in the progressive increase and decrease in the spacing ratio. In addition to drag coefficient, the hysteresis is present for Strouhal number as well. There is only one significant jump for the hysteresis in Strouhal number and this jump is lower spacing limit of regime. As the spacing ratio goes beyond the upper limit of hysteresis regime, the amount of Strouhal number increases for the higher Reynolds number. Increasing the Reynolds number to 8000 and 16000 in the Mode II flow pattern result

in the weaker vortex shedding from the first cylinder, and decrease in the fluctuating pressure coefficient on the side and rear face of the first cylinder and on the front and side face of the second cylinder. As the base pressure increases the drag coefficient differences decreases between Mode I and Mode II.

S. C. Yen et al. [10] did experimental investigations on two square cylinders in tandem arrangement in a vertical water tunnel at low Reynolds numbers. They categorize the flow into three categories by the aid of the particle image velocimetry (PIV) scheme as the spacing ratio between the cylinders and Reynolds number changed. The first flow pattern was the vortex sheet of single mode as it resembles the single cylinder model. The reattachment of the vortices as the cross-section of the downstream cylinder is associated with the vortex sheet of reattach mode which is the second flow pattern. And the last observed pattern was the vortex sheet of binary mode which is associated with co-shedding. As they concluded, at very low Reynolds number the Strouhal number decreases as the Reynolds number increases. But for the higher range of Reynolds number, Strouhal number increases as the Reynolds increases, and the Strouhal number will reaches the relatively constant value as the Reynolds get even higher.

Dependency of Strouhal number on the spacing ratio of two inline circular cylinders and Reynolds number was examined by G. Xu and Y. Zhou [11]. They carried out their investigation in a closed-circuit wind tunnel, at $800 - 4.2 \times 10^4$ Reynolds. The vortex shedding frequencies were measured by the aid of two hot wires located behind each circular cylinder. Laser-induced fluorescence (LIF) technique was used in the water tunnel to visualize the flow. They found the Strouhal number in the strong dependence with the spacing ratio and Reynolds number. The relationship between the Reynolds

number and Strouhal number were divided into four different groups as the spacing ratio changes. There is a spacing ratio, called critical spacing ratio, which there exist no vortex shedding behind the upstream cylinder as the spacing ratio is less than the critical value, and there are vortex shedding from both cylinders simultaneously when the spacing ratio is greater than the critical value. When the gap ratio is between $1-2$, the shear layers were separated at the first cylinder and the vortices were formed behind the second cylinder. As the gap ratio increases and examined in the range of 2 and 3, there exist transition from the formation of vortices behind the second cylinder to the reattachment of the separated shear layers on the second cylinder. The presence of another transition regime from the reattachment to co-shedding was observed, as the spacing ratio was in the range of $3-5$. The final regime is associated with the shedding of vortices from both cylinders at the same time for the spacing ratios greater than 5. According to the authors observations, when the Reynolds is greater than 2×10^4 the Strouhal number appears to be relatively constant for a given gap ratio. They also found out the critical Reynolds number decreases for the transition regimes as the spacing ratio increases.

Another experimental study was carried out by Chin_Yi Wei and aJeng_RenChang [12] on the flow properties of wake and base bleed flow downstream of two bluff bodies arranged side by side. Two dimensional flat plates, square cylinders and circular cylinders were the adopted bluff bodies. Their investigations were divided into two different parts. For the first part, the biasing behavior and flow characteristics of two body arrangements with the same cross sectional dimensions but with different vortex shedding frequencies but with different cross sectional dimensions. Their tests were

executed in a close return type low speed wind tunnel and the flow visualization was performed by the aid of water table. The Reynolds number for these investigations ranges from 4000 to 6000. Authors pointed out that, for the case of same cross sectional dimensions, the vortex shedding frequency downstream from two side by side bodies is about the half of the average of the shedding frequency for each single body when the gap distance is small. As the gap ratio increases to the distance which called large related to the geometry of bluff body adopted, the vortex shedding frequency reaches asymptotically to the value of single body condition. Analysis of biasing behavior of the flow revealed that the gap flow leans to deflect toward the narrow wake side downstream of two bluff bodies in side by side arrangement. They also observed the relatively unstable biasing characteristic of gap flow when the widths of the wake downstream of each bluff body were almost same.

Coherent and incoherent flow structures in wake of bluff bodies were another area of flow characteristics that attracted attention for over four decades. Cetin Mazharoglu and Hasan Hacisevki [13] did some experimental investigations in the open type low speed wind tunnel to analyze the periodic unsteady flows behind a single plate, as well as the double plate in tandem arrangement [14]. The free stream velocity was adjusted at $16.4 \pm 0.02(m/s)$ and kept constant. The tests were done at Reynolds 33000. Phase averaging methods were used to analyze the data together with triple decomposition technique. Dimensions of the single flat plate were selected in the way that could be compatible with the previous works. So, the ratio of thickness to width was 0.2 or 20%. Their obtained values were consistent to within $\pm 5\%$, with the work of Kiya and Matsumara [15]. According to authors as the distance from the rear face of the flat plate

increases the wake behind it widens and the stream wise velocities decrease to maintain the continuity. The computed values of the case of single plate were compared with the case of two in line plates, with different gap ratios. The stream wise velocity contours, coherent velocity contours and incoherent velocity contours, were depicted at the same distance from the rear face of single plate and the rear face of the downstream plate for the case of double plates. Theratio of gap between the plates to the width of the flat plates for tandem plates, were taken at 0.5 and 1.0. The graphs of the velocity contours showed the similar patterns, but the peak value of single plate was as high as 15% in compare with the double plates. Contours of coherent velocity were almost same for all cases, but the magnitude of the peak values were reduced 12% from single plate to double plate with the gap ratio of 0.5 and arise 12% from single plate to the case of 1.0 gap ratio. Finally, the peak values of the incoherent flow structures of the single plate was achieved 70% and 40% higher than the values of tandem plates with 0.5 and 1.0 gap ratio, respectively.

F. Auteri et al. [16] performed an experimental investigation on two normal flat plates in tandem arrangement to check the dependency of the flow on the separation between the plates. As they stated there are two different flow regimes as the distance between the plates change. There is also a small interval of separation that both flow regimes are available and change periodically. To get such conclusion the test was executed in an open loop wind tunnel, with turbulence level as low as 0.3%, and 10% solid blockage. The study was done by means of a constant temperature hot wire anemometer and oil smoke visualization at $Re = 8340$. The narrow interval of separation where both flow regimes can be observed is called ‘critical separation’. In this region the wake behavior

changes abruptly and the presence of a maximum Strouhal number is almost same as the Strouhal number for the single plate. As the separation increases from the critical separation, the Strouhal number decreases dramatically to reach its minimum. As the separation distance passes this point it starts increasing slowly to gain the near single plate value as expected. F. Auteriet et al. concluded that the first flow regime exists when the plated are closed to each other ad at this point the flow properties slightly are related to the Reynolds number. They also mentioned that as the Reynolds number increases the critical separation value increases as well. For the small separation, since there is no enough space for the vortex formation the separated shear layers transit the dead flow region and start shedding behind the downstream plate. This situation is called "one body mode". For the case of large separation the vortex shedding phenomena is visible behind both upstream and downstream plates. "Dual body mode" is denominated for this case. As a result the shedding frequency depends on the gap vortex dimension as uttered by authors. Also, the changes in Strouhal number depend strongly on the plate separation as it was showed by authors and mentioned in literature.

2.3 Validity of Numerical Analysis in Comparisons with Experiments

Numerical study and the comparison between the results from the numerical and experimental researches are presented in this section. These comparisons have been done to check the eligibility of different numerical methods to apply in different research areas. These efforts made to improve the existed methods or to create new methods.

Gerhard Bosch and Wolfgang Rodi [17] simulated the flow past on square cylinder, which was located at different distance from adjacent wall, at $Re = 2.2 \times 10^4$ to check the validity and accuracy of numerical method. Equations of two-dimensional $(2 - D)$

unsteady flows were solved together with two versions of $k-\varepsilon$turbulence model, since the presence of superimposed turbulent fluctuation on the flow in sensible. The standard $k-\varepsilon$ model provide the extensive turbulent kinetic energy in the stagnation region, so as authors stated when the cylinder is relatively close to the wall this model showed steady solution which is in disagreement with the available experiments in the literature. The simulation was performed with modified $k-\varepsilon$ model, (Kato and Launder) which eliminates the unusual production of turbulent kinetic energy. As demonstrated by Gerhard Bosch and Wolfgang Rodi, the vortex shedding production of this modification is in agreement with experiments. As the square cylinder was adjusted closer to the wall, both turbulence models got the steady state solution which was compatible with the experimental findings. Increasing the gap resulted in the formation of the vortex shedding from both versions of $k-\varepsilon$ models. The shedding for the case of standard $k-\varepsilon$ model was much more damped.

They expressed their main conclusion in the way that "the modification of Kato-Launder improves significantly the predictions of vortex shedding flow past a square cylinder also in the presence of an adjacent wall."

Unclear points on the applicability of numerical methods caused KatsuyaEdamoto and Mutsuto Kawahara [18] to do two- (2-D) and three-dimensional (3-D) numerical analysis on the flow around two in-line square cylinders. Finite element analysis was performed for the some range of spacing ratio between the cylinders and for the various Reynolds numbers. The numerical results were compared with wind tunnel results. They interpreted their data by the aid of the time-averaged pressure coefficient graphs at various Reynolds number. According to their findings, the computed time-averaged

pressure coefficient was not in the good agreement with the experimental data as the shedding of strong vortices behind the cylinders was observed independent from widely changed Reynolds. The authors stated that the 2-D analysis is congruous with the experimental data as the spacing ratio between the cylinders was wide or narrow enough. 3-D computation was found to be consistent with experimental results at Reynolds 10,000. 3-D analysis determined as an effective way to interpret the data in this area.

Jiunn.Chi Wu and Young.Chun Hu [5] did the numerical study on the wake of two circular cylinders with same cross sectional area in both inline and tandem arrangement. The investigation was done for different spacing ratios between cylinders varying from 1.5 to 4.0. Finite difference method was selected as a solution for unsteady Navier-Stokes equations in terms of stream function and vorticity formulation. The flow was simulated at$Re = 200$. The results of their simulation were expresses for different spacing ratios. When the ratio of the longitudinal spacing between cylinders center (L) to the cylinder diameter (D) is equal to 1.5 $(L/D = 1.5)$ cylinders are relatively close to each other. At this step for inline cylinders they act more like a single body. Shear layers separated from the front cylinders and reattached to the rear cylinder. Two cylinders act as an elongated body which results in enclosure of cylinders by shear layers. A regular vortex shedding can be seen behind the second cylinder. They also, mention that "flow motions inside the interspace of two cylinders are not stagnant." As L/D increases to 3.0, periodic vortices start forming from two separated shear layers from the upstream cylinder, and reattach alternately at the rear cylinder. Jiunn_Chi Wu and Yung-Chun Hu yield the regular vortex shedding from each cylinder as the spacing ratio exceed 3.8.

Despite of simultaneous vortex shedding from both front and rear cylinders the characteristics of surface pressure, vortex shedding and aerodynamics forces of two cylinders are markedly different. The relationship between the drag coefficient and spacing ratio was also of their concern.

As the gap ratio increases, the amount of drag coefficient decreases for the front cylinder, while the drag coefficient of rear cylinder increases. The numerical results of their study was compatible with the pervious experimental works (Ishigai, et al., [19]; Zdravkovish ,[20] and Bearman and Wadcock [21]) for the gap ratio smaller than the critical value. (Critical spacing was taken at $L/D = 3.4 \sim 3.8$ as reported in experiments. The computed drag coefficient of the upstream cylinder was greater than the other experimental and numerical data.

Large eddy simulation (LES) model applied by Chen. L. et al., [22] to analyze the formation and the convection of vortices behind two cylinders arranged side-by-side. Finite element method employed on an unstructured mesh that consisted of hexahedral elements to come through the solution to the three-dimensional Navier-Stokes governing equations. Prediction of the wake dynamics elucidated at Reynolds 750 for two different spacing ratios, the large ratio and the intermediate one. For the case of large spacing ratio, the formation of two symmetrical wake streets observed which is in the agreement with experimental results. As the ratio decreases to some intermediate value, the tendency of gap flow to "flip" observed. Gap squeezing effect and merging the generated vortices behind the cylinders can explain the gap flow behavior. The gap flow deflection that obtained from the numerical simulation was compatible with the experimental observations.

N. N. Mansour et al. [23] simulated the flow fields from a turbulent channel to determine the turbulent kinetic energy (k) and dissipation rate (ε) profiles. Two-equation $k-\varepsilon$ model was used to imitate the flow to interpret the dependency of the eddy viscosity damping function on the both Reynolds number and distance from the wall. The authors stated that the existing transport models must be improved in the near wall region.

Long time-scale simulations, of vortex shedding in unsteady flow past a thin plate placed orthogonal to the flow direction, were performed by H.R. Tamaddon et al. [24] to check the validity of Taylor-Galerkin/pressure-correction finite element algorithm for solving the transient Navier-Stokes equations and complex unsteady problems. The flow characteristics were studied at Reynolds 1.2625×10^5 and 500. The investigations were done in two different cases, unperturbed flow and perturbed flow. According to observations flows started from steady state and after some time the vortex shedding phenomenon occurred. This phenomenon happened for both unperturbed and perturbed flows. The flow perturbations were done, firstly by positioning the plate vertical to the flow direction and moving it upward by half of a plate size and then moving it down and downer, again by the half of the plate length. Changing the inlet boundary conditions in a way to set the velocity of half the inlet nodes equal to zero and the rest of nodes equal to twice the free stream velocity is the second way to apply perturbations on the flow. As H.R. Tamaddon Jahromi et al concluded the vortices started shedding in the first approach of perturbed flown 200 seconds sooner than the case of unperturbed. And this matter happened some300 seconds sooner in the second approach of perturbation in compare with the first approach. They also mentioned that these disturbances have no

effects on the shedding frequency, and the Stnumber computed from the periodic shedding was same with the case of unperturbed flow as expected. The results of this study are compatible with the previous results of the experimental investigation, numerical results and pictorial results. So, they found their method, obviously capable of solving problems engaged with long time scales of operation, and determined it as a powerful tool to analyze such unsteady problems.

Unsteady flow behind a flat plate located perpendicular to the flow direction was simulated by D.S. Joshi et al., [25]. This numerical investigation carried out by integrating the three-dimensional unsteady Navier-Stokes equations. Second order accuracy in time and space were considered in a finite-volume numerical scheme. The three-dimensional results were compared with the comparable two-dimensional at Reynolds 1000. Obvious differences between the two-dimensional and three-dimensional results were observed. The computed value for the drag coefficient in 2-D analysis oscillates at twice the vortex shedding frequency with the higher mean value than the obtained value from experiment. But in three-dimensional analysis this value is relatively close to the experimental value. The mean velocities are compatible with the experimental results, but the root mean square (rms) quantities are slightly higher than the experimental values. According to researchers the three-dimensional simulation seems more suitable for the interpretation of flow in this area.

Robert N. Merney et al. [26] executed experimental and numerical simulations on the flow and dispersion of gasses, released by the sources in the vicinity of the different building shapes. These studies were done in various wind tunnels for the experimental part of the research and the numerical analysis were fulfilled by FLUENT and

FLUENT/UNS utilizing standard$k-\varepsilon$, RNG$k-\varepsilon$, and Reynolds stress model (RSM) approximations. The results from the both sections were compared to check the eligibility of turbulence model for this case. According to the researchers, the RSM turbulence model gave the more realistic results in comparison with the standard and RNG $k-\varepsilon$ models.

H. M. Skye et al. [27] provided the study on the vortex tube by the aid of both computational fluid dynamics and experimental measurements which taken by applying a commercially available vortex tube. Two-dimensional, steady axisymmetric model simulated by two turbulence model, the standard and renormalized (RNG) $k-\varepsilon$ models, specially, to measure the inlet and outlet temperature of the tube. Experimental and computational results were compared, and the successful use of CDF in this regard confirmed. As a result, CFD can be used as a powerful tool which has the ability to optimize the vortex tube design.

As it was mentioned in the introduction part of this chapter the numbers of researches on the comparison between the experiments and CFD results are the strong reasons to make the use of this new technology as a necessary part of each research to minimize the restrictions of CFD.

Chapter 3

METHODOLOGY

3.1 Introduction

This numerical study was carried out to check the validity of specific turbulence models in the computational fluid dynamics (CFD) in the wake of bluff bodies, together with the effects of variation in the spacing ratio between the bodies on the fluid manner. The quantitative investigation performed on the wake properties of the two dimensional flow, past from two normal flat plates in tandem arrangement, and a square cylinder by means of finite volume method. Control volume technique applied to convert the partial differential equations to the algebraic ones to solve them numerically and reach the solution which is capable of satisfying the governing equations in every single element of the grid. This numerical study used the visualization of CFD data techniques by the aid of its graphs and charts to analyze the flow characteristics in order to compare the results with the previous experiments. To make the results of this empirical study comparable to the previous experiments, Hasan Hacisevkis's experiment [28] (Appendix A) was taken as a reference. He did his experimental investigation in an open type low speed wind tunnel with a working test section of dimensions $0.5 \times 0.5\, m^2$ and of length $1.5\, m$. Two flat plates were located normal to the wind direction in the tunnel as vortex shedders with $30mm$ width, $500mm$ height and $6mm$ thickness dimensions. A square cylinder unaccompanied with any other model with dimension of $30 \times 30\, mm^2$

and of $500mm$ height was allocated in the wind tunnel as well. The initial conditions of the mentioned experiments such as the velocity inlet, pressure of the system and etc. were assumed as input data for the numerical investigation. This study was performed in three steps: pre-processing by Gambit 2.2.30® and ANSYS/FLUENT 13.0® commercial grid generator and codes respectively, processing with ANSYS/FLUENT13.0® and finally post-processing by ANSYS/FLUENT13.0® and Tecplo 360 2010®. These steps have been explained in detail in this chapter.

3.2 Pre-Processing

3.2.1 Geometry Modeling and Grid Generation

Since, all the selected bodies as vortex shedders were long in one direction and the cross-sectional area in that direction was constant and there was no significant variation in that direction and the flow was normal to the body, the problem could be completely described in one plane, which made it as two dimensional model [29]. The bottom-up approach was used to create the model geometry. Vortices generated as low dimensional entities and then lines and faces created top of them as higher dimensional entities. The wind tunnel was specified to be huge enough to be reconciling with the model to prevent the effects of wall interference and blockage to the geometry. Blockage which is the ratio of the frontal area of the model to the test section must be less than 7.5% as indicated by [4] and less than 5% as mentioned by [30]. According to the mentioned explanations the wind tunnel was drawn as a two-dimensional rectangular geometry with $1.5m \times 0.5m$ dimensions. Two flat plates with $30mm$ width and $6mm$ thickness were located inside the rectangle. The spacing between the plates was determined by different gap ratios. Gap ratio determined as non-dimensional ratio which is the ratio of gap

between the plates to the width of the plates g/d. The gap ratio ranges from 0.3 to 2.0 in this study. All of these drawings were performed in Gambit2.2.30® program. As the geometry modeling completed, the pre-processing moved to its next step which was grid generation.

The meshing defined, according to the aim of the project and the way that flow supposed to be analyzed. Grid generation is the most important part of CFD problems which needs the high resolution in the locations that the act of flow is more sensitive in order to reduce the error, memory wasting and the convergence time. High density mesh was required in the boundary layers, the separated region and the wakes since, the viscous and rotational effects are significant in those areas. The grids must be fine sufficiently to resolve the flow. In order to save time and memory, the number of elements or control volumes, that are available far, from the plates and wake of the bluff bodies, were much lower than the number of elements in complex part of the problem. Unstructured quadrilateral grid technology was considered with presence of mixing element type. Paving for the creation of quads in 2-D was executed automatically. The measurements of the grid quality are not absolute but they could help the grid improvements. The quality of mesh can be checked in both Gambit 2.2.30® and ANSYS/FLUENT 13.0® programs.

Different terms are available to show the mesh quality by their quantities such as skewness, aspect ratio and orthogonal quality. The maximum acceptable value of the skewness quantity is 0.5, the lower the skewness, the better the mesh quality. ANSYS/FLUENT 13.0® is also capable of checking the mesh quality, but before that

the boundary zones must be defined in Gambit 2.2.30®. There are three different types of boundary zones; velocity inlet, out flow and wall.

At this level, the model is ready to be read by the ANSYS/FLUENT13.0®. The first action to take is to check the mesh quality. The program warns if there exists any problem. The orthogonal quality ranges from 0 to 1, the closer the orthogonal quality to 1, the better the mesh quality. All of the meshes that imported to this program had the orthogonal quality equal or greater than 0.92.

3.2.2 Problem Set Up

The solution of the CFD models rely on the governing equations of the fluid flow which are the mathematical statements of the conservation laws of physics. The CFD program has been designed to obey these rules that have been presented here while analyzing the fluid flow [31];

- The mass of fluid is conserved which means the rate of increase of mass in fluid element is equal to the net rate of flow of mass into fluid element (continuity equation is the mathematical statement of this law),

  $$\frac{\partial \rho}{\partial t} + \frac{\partial (\rho u)}{\partial x} + \frac{\partial (\rho v)}{\partial y} + \frac{\partial (\rho w)}{\partial z} = 0 \qquad (3.1)$$

  Where,

  $\rho$is density of the fluid,

  u, v, w are the velocities in x, y and z direction, respectively.

- The rate of change of momentum equals the sum of the forces on a fluid particle (Newton's second law),

$x-$Momentum:

$$\frac{\partial(\rho u)}{\partial t} + div(\rho u \boldsymbol{u}) = -\frac{\partial p}{\partial x} + div(\mu\ gradu) + S_{Mx} \quad (3.2)$$

$y-$ Momentum:

$$\frac{\partial(\rho v)}{\partial t} + div(\rho v \boldsymbol{u}) = -\frac{\partial p}{\partial y} + div(\mu\ gradv) + S_{My} \quad (3.3)$$

$z-$ Momentum:

$$\frac{\partial(\rho w)}{\partial t} + div(\rho w \boldsymbol{u}) = -\frac{\partial p}{\partial z} + div(\mu\ gradw) + S_{Mz} \quad (3.4)$$

Where, $P =$ Pressure,

$\mu =$ The first dynamic viscosity,

S_{Mx}, S_{My}, S_{Mz} are total force on the element due to body forces in x, y and z directions, respectively.

- The rate of change of energy is equal to the sum of the rate of heat addition to and the rate of work done on a fluid particle (first law of thermodynamics).

$$\rho c_p \left(u\frac{\partial T}{\partial x} + v\frac{\partial T}{\partial y} + w\frac{\partial T}{\partial z}\right) = \beta T \left(u\frac{\partial P}{\partial x} + v\frac{\partial P}{\partial y} + w\frac{\partial P}{\partial z}\right) + div(k\ divT) + \boldsymbol{\Phi} \quad (3.5)$$

Where, $c_p =$ Specific heat at constant

$T =$ Temperature

$\beta =$ Coefficient of thermal expansion

$\boldsymbol{\Phi} =$ Dissipation function

$$\Phi = 2\mu\left(\frac{\partial u}{\partial x}\right)^2 + 2\mu\left(\frac{\partial v}{\partial y}\right)^2 + 2\mu\left(\frac{\partial w}{\partial z}\right)^2 + \mu\left(\frac{\partial v}{\partial x} + \frac{\partial u}{\partial y}\right)^2 + \mu\left(\frac{\partial w}{\partial y} + \frac{\partial v}{\partial z}\right)^2 + \mu\left(\frac{\partial u}{\partial z} + \frac{\partial w}{\partial x}\right)^2 + \lambda\left(\frac{\partial u}{\partial x} + \frac{\partial v}{\partial y} + \frac{\partial w}{\partial z}\right)^2 \quad (3.6)$$

Where, λ is the second coefficient of viscosity.

The generic settings of the problem, which are related to the solver, could be defined at this stage. Compressibility is one the factors that has impact on the selection of the solver type. In general, two solver methods are available, the pressure-based and density-based solvers. As the Mach number, the dimensionless quantity which is, the ratio of fluid flow velocity to the speed of sound was less than 0.3 the flow could be treated as incompressible and the density changes were negligible. For the incompressible and low Mach number flows, pressure-based solver seems the suitable selection. The relative velocity formulation was preferred over the absolute one optionally since, for velocity inlets there is no difference between these two formulation types. Transient solution was accounted since the vortex shedding is a time dependent phenomenon and the planar option which indicated that the problem was in 2-D, was selected.

3.2.3 Turbulence Modeling

The proceeding step was the determination of the viscous model for this flow. Generally, there are three kinds of viscous model; inviscid, laminar and turbulent, and the selection of them depends on the value of Reynolds number. The formation and shedding of circulating fluid chunks as the flow passed from long cylinders are called vortices, for Reynolds greater than 90 (the Reynolds number for the under investigation flow is 33000). Velocity fluctuations caused by vortices result in the rise in additional stresses on the fluid which are called Reynolds stresses that could be simulated by the

turbulent viscous model. More transport equations must be solved as the flow become turbulent to represent the turbulent properties of the flow. Different types of turbulence models are available in the ANSYS/FLUENT 13.0 ® program that is presented in the Appendix E. These models are classified according to the presence of transport equations in each model. Unfortunately, there is no single turbulence model that is universally accepted to be superior for all classes of the problems. Different parameters, such as the physics covering the flow, the available amount of time, the required level of accuracy and the computational resources that are present, have effects on the choice of turbulence model. And understanding the capabilities and limitations of the various options could lead selecting the most appropriate model. The $k-\omega$ shear-stress transport (SST) model and the linear pressure-strain Reynolds stress (RSM) model were selected for this problem.

The $k-\omega\ SST$ model is the 2-equation model which is the combination of $k-\omega$ and $k-\varepsilon$ models that could get use of the power points of each model for near walls and far from walls, respectively. This model consists of two transport equations for the turbulence kinetic energy k and the specific dissipation rate ω which are represented in the Appendix D.

The $k-\omega\ SST$ model is good in predicting the adverse pressure gradients in boundary layers and separating flows. And there is no need to model any extra damping functions as they could be used as a low-Reynolds turbulence models. These reasons together with, the robustness and widely usage of this turbulence model in aerodynamic flows caused the utilization of this model in this study.

The RSM turbulence model consists of five transport equations in 2-D flows which are the transport equations for the Reynolds stresses together with one equation for the dissipation rate. The main purpose of applying the RSM model as a viscous model was the direct computation of the Reynolds stresses in its approach. Reynolds stresses $u'^2, v'^2, u'v'$ could be assessed by the aid of this model. Pressure-strain Reynolds stress (RSM) model together with the enhanced wall treatment (EWT) approach performed to calculate the Reynolds stresses. The transport equations used for this model have been presented in the Appendix D.

The pressure gradient effects option were also enabled as the enhanced wall treatment options to give more accurate results in wall boundary layers.

Since there is no variation in density of the flow, there is no relationship between the energy equation and conservation of mass and momentum. But the option which enables the calculation of the energy equation was turn on in order to get information in the energy regard.

3.2.4 Initial and Boundary Conditions

The next step was to define the initial and boundary conditions of the CFD problem which are important to be represented accurately in the computational model. The boundary conditions were used by ANSYS/FLUENT 13.0® to figure the mass flow into the domain, fluxes of momentum, energy, and species through the inlet. As it was mentioned, three boundary zones were identified in the Gambit 2.2.30 ® program. The initial conditions of this study are same as the available data from the experiment that was under investigation. In the velocity inlet boundary zone the magnitude of the air

velocity was considered as $16.4 \pm 0.02(m/s)$ normal to the boundary and in x-direction. The turbulence specification method specified 0.8% turbulent intensity together with $0.0021\ (m)$ turbulent length scale. The initial temperature was taken at $289.75K$. No slip conditions were determined for the walls that were stationary. And the flow rate weighting was considered as 1 since there was only one outflow boundary zone.

3.3 Processing

The success in the CFD can be determined by three mathematical concepts called, convergence, consistency and stability. Solution setup and the calculation tasks are designed at this part to satisfy these considerations. The convergence is defined as a property of numerical method that reaches the exact solution as the spacing of grid decreased to zero. In other word, the model is mathematically converged as the values of the entire under investigation domain experience no significant changes from the present iteration to the next. Consistency in numerical schemes results in the formation of systems of algebraic equations that are in the same way as the original governing equations as the grid spacing diminishes to zero. The last mathematical concept which deals with damping the errors as the problem is in its processing level is stability.

3.3.1 Spatial Discretization Scheme

The convergence speed and the requirement for the memory of the coupled algorithm are much higher than the segregated one. According to the size of the mesh and the available memory of the computer, the segregated algorithm was preferred over the coupled algorithm for the pressure-velocity coupling method in the pressure based solver. The ANSYS/FLUENT13.0® program is capable of performing three segregated

velocity-coupling algorithms. The Pressure-Implicit with Splitting of Operators (PISO) was selected over the other pressure-velocity coupling schemes as it is recommended for all transient flows. This scheme is based on the higher degree of the approximate relation between the corrections for pressure and velocity. The PISO algorithm developed two additional correction, neighbor correction and skewness correction, to improve the efficiency of the calculation of momentum. Momentum correction or "neighbor correction" decrease the number of repeated calculations, in the solution stage of pressure-correction equation, required by other pressure-velocity coupling schemes to satisfy the continuity and momentum equations more closely. The PISO algorithm consumes more CPU time per solver iteration and diminishes the number of iterations to achieve the convergence. Another iterative process similar to the neighbor correction is required to identify the components of the pressure-correction gradient as they are not known on cell faces. This process is called "skewness correction" reduces the problems associated with convergence with highly distorted meshes. One more iteration of skewness correction executed over the neighbor correction for each separate iteration to obtain high accuracy adjustment of the face mass flux correction in the normal pressure correction gradient.

Discretization schemes were identified to solve the convection and diffusion terms in the equations deal with the conservation laws of physics. The least-squares cell-based method was utilized as a solution to the gradients. This method has been chosen because of its high accuracy and low cost (in terms of computation) and its capability to perform on unstructured meshes. The "standard" method was applied for the pressure interpolation scheme as it is acceptable for most cases. The second order upwind

discretization was selected for the momentum and energy equations because of the more accurate results that are obtained from this scheme. Transient formulation was created according to the iterative time-advancement scheme. This method solves each equation for a defined time step, iteratively to meet the convergence criteria. As a result, numbers of outer iterations are required for each time-step. The bounded second order implicit was selected as transient formulation, which provides better stability than the other formulations. The bounded second order is in alignment with the second order implicit in terms of accuracy.

The under-relaxation factors, which have been related to each quantity of the transport equations, together with time-step size are the other parameters that have effect on the convergence difficulties. The under-relaxation factors are identified to be close to the optimal values to speed up the convergence. The slight changes in these factors result in the changes in convergence speed. Relatively small step size $(2e-4\,second)$ was accounted for the time-step size to meet the convergence and stability criteria. The absolute convergence criterion which compares the residual of each equation in iteration with a user specified value at the initialization part was selected together with the scaled residual. The required level of residual, changes according to the specified model. The data was auto-saved each 100 time steps to have the changes in each$0.02\ second$.

3.4 Post-Processing

The final level of the CFD program is the post processing which describe the flow behavior by the aid of graphs, reports and charts. Reports can help to understand how the program is proceeding, for example the values of mass flow rate must be equal in

magnitude at inlet and outlet boundaries which is obtained in all analyzed models in this report.

3.5 Verification of CFD Codes

As the residual monitored in the program, the convergence of iterations in each time steps were illustrated which is the expression of satisfying the convergence concept. The conservation laws of physics were satisfied which shows the consistency in the results.

3.6 Limitation of Research Methodology

A major limitation to this study proved to be the lack of the powerful computers and time.

Chapter 4

RESULTS

4.1-Introduction

The use of CFD and the comparison with experimental data to verify the validity of the technique which is the aim of this study is carried out as follows:

- The available experimental data are the results of study on the two coherent and incoherent structure of flow behind two tandem flat plates.
- CFD analysis were carried out on the same problem with following gap ratios:

$g/d = 0.3, 0.5, 0.6, 1.0, 1.8$ And 2.0

The results of this study are covered in the following:

- From the above study the results for the gap ratios of 0.5, 1.0 and 2.0 could be compared with the available experimental data which is presented in the following sections. This comparison proves the ability of the CFD technique in similar studies.

4.2 Analysis Results

The software employed for the analyses as mentioned before, is the ANSYS/FLUENT 13.0®. This powerful software produces many useful outputs that consist of graphical forms giving deep understanding of the flow behavior. The analysis covers the study of

flow around bluff bodies with six different gap ratios. Presenting all the outputs for all cases is avoided but in the case of 0.3 gap ratio, which was analyzed by $k-\omega\ SST$ model as most cases, thirteen graphical outputs are presented as follows:

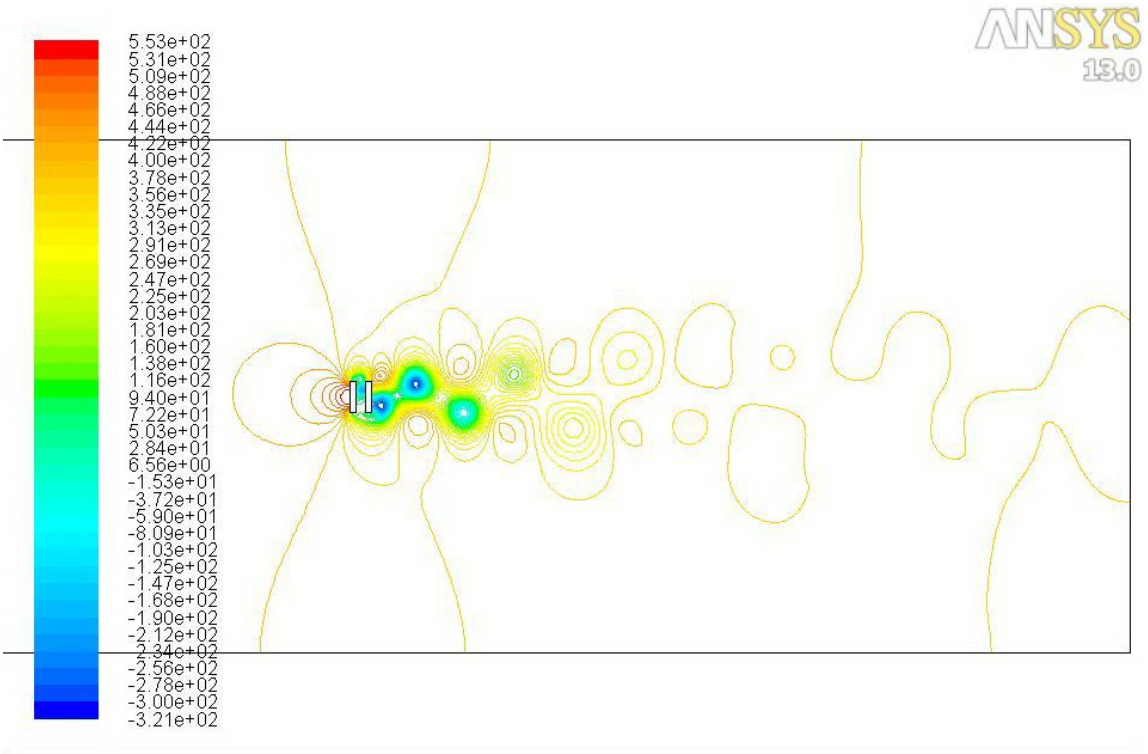

Figure 1. Contours of Static Pressure (Pa), at $g\ /\ d$=0.3

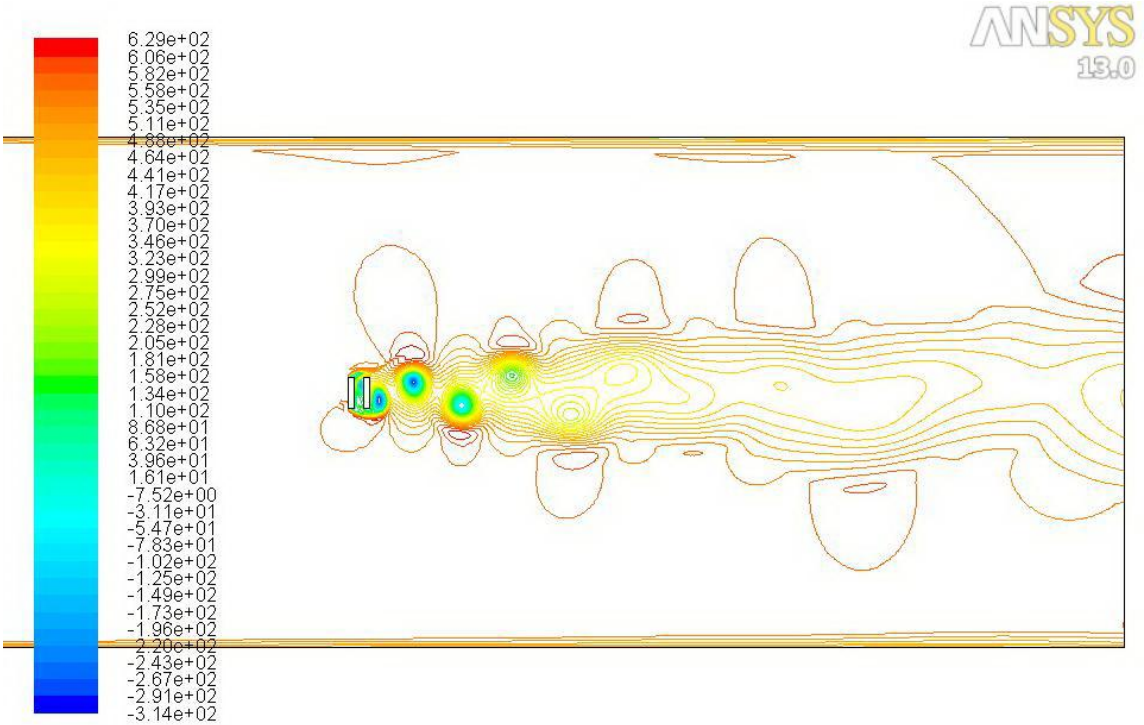

Figure 2. Contours of Total Pressure (Pa), at $g\ /\ d = 0.3$

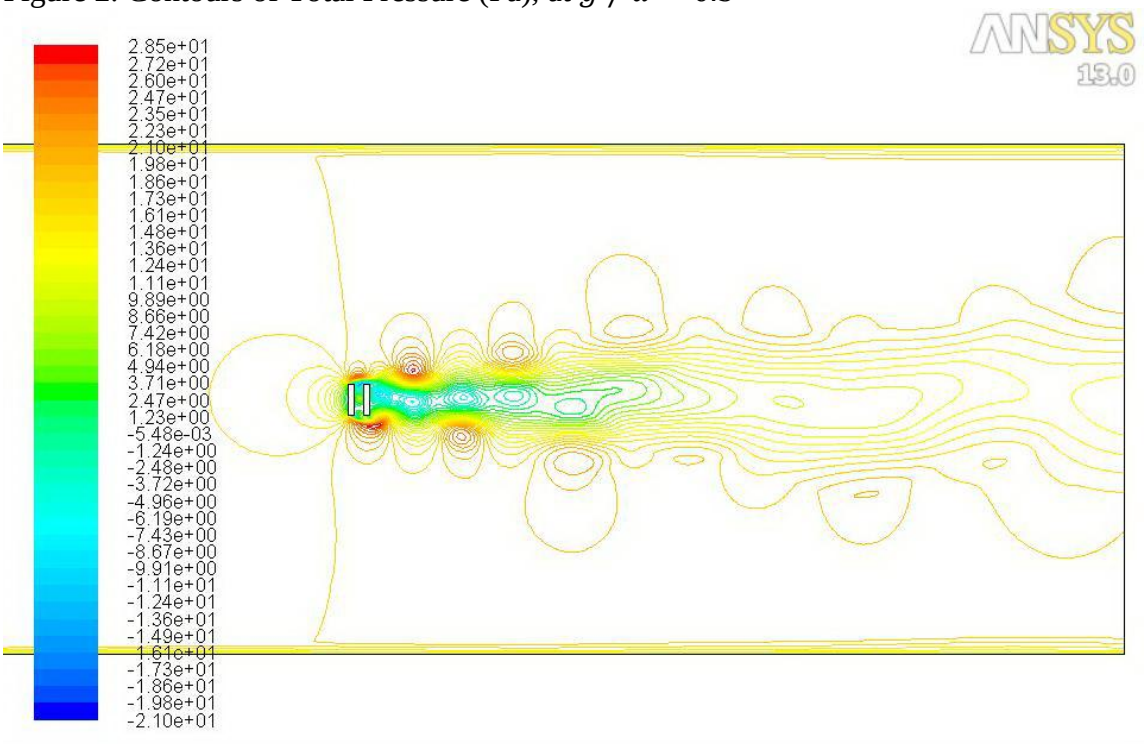

Figure 3. Contours of X-Velocity $(m\ /\ s)$, at $g\ /\ d = 0.3$

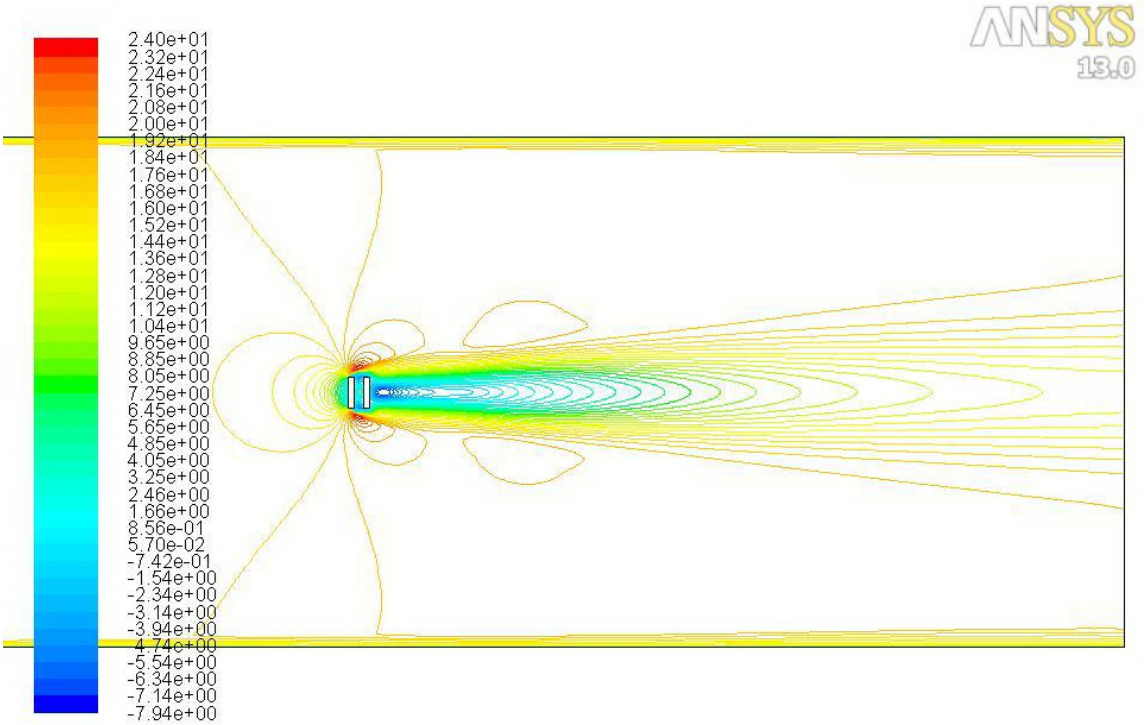

Figure 4. Contours of Mean X-Velocity ($m\ /\ s$), at $g\ /\ d = 0.3$

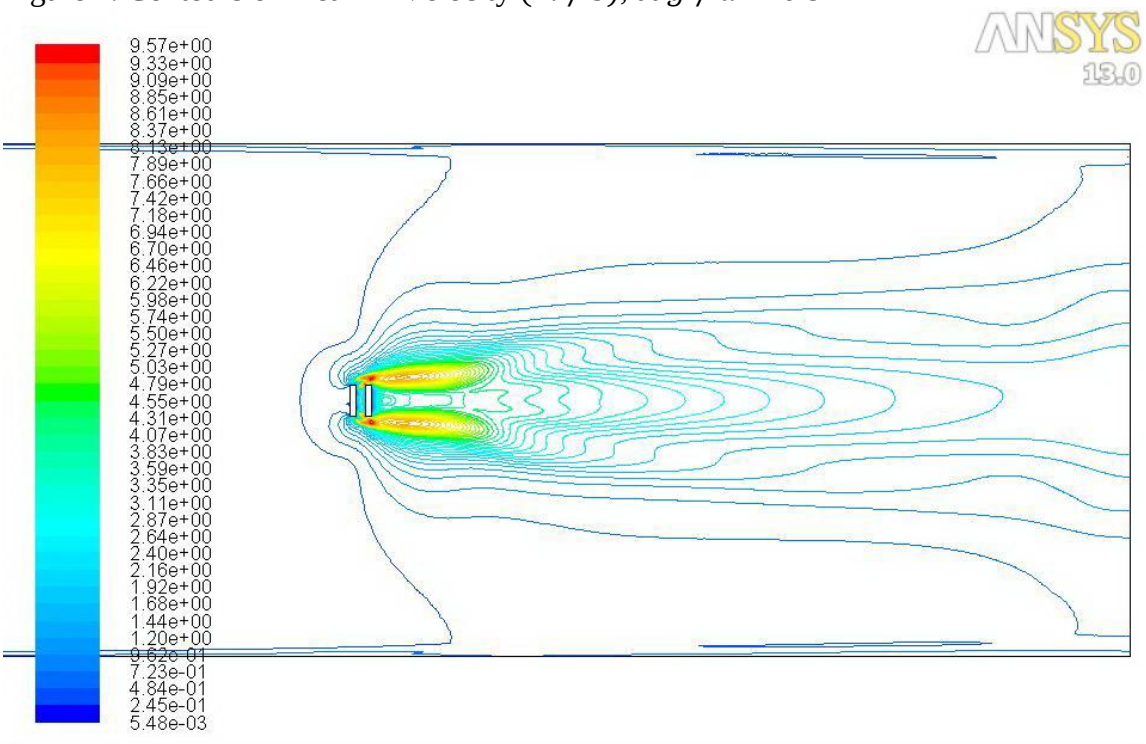

Figure 5. Contours of RMS X-Velocity ($m\ /\ s$), at $g\ /\ d = 0.3$

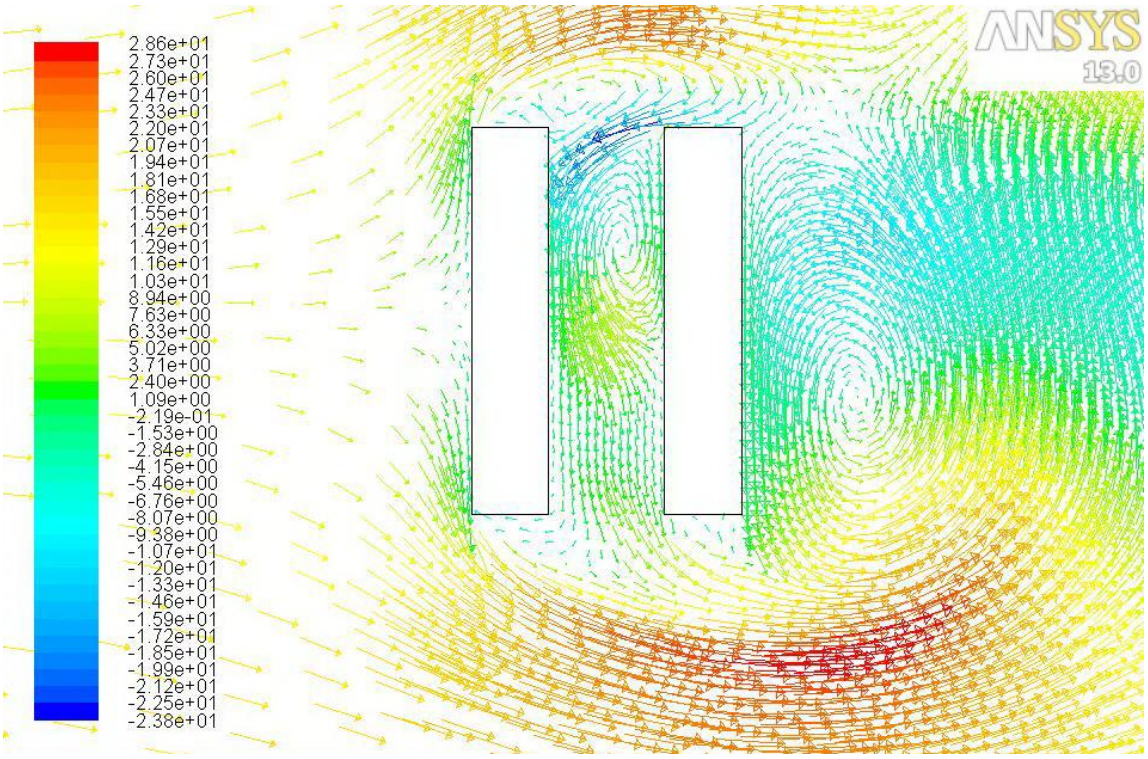

Figure 6. Velocity Vectors Colored by X-Velocity ($m\ /\ s$), at $g\ /\ d = 0.3$

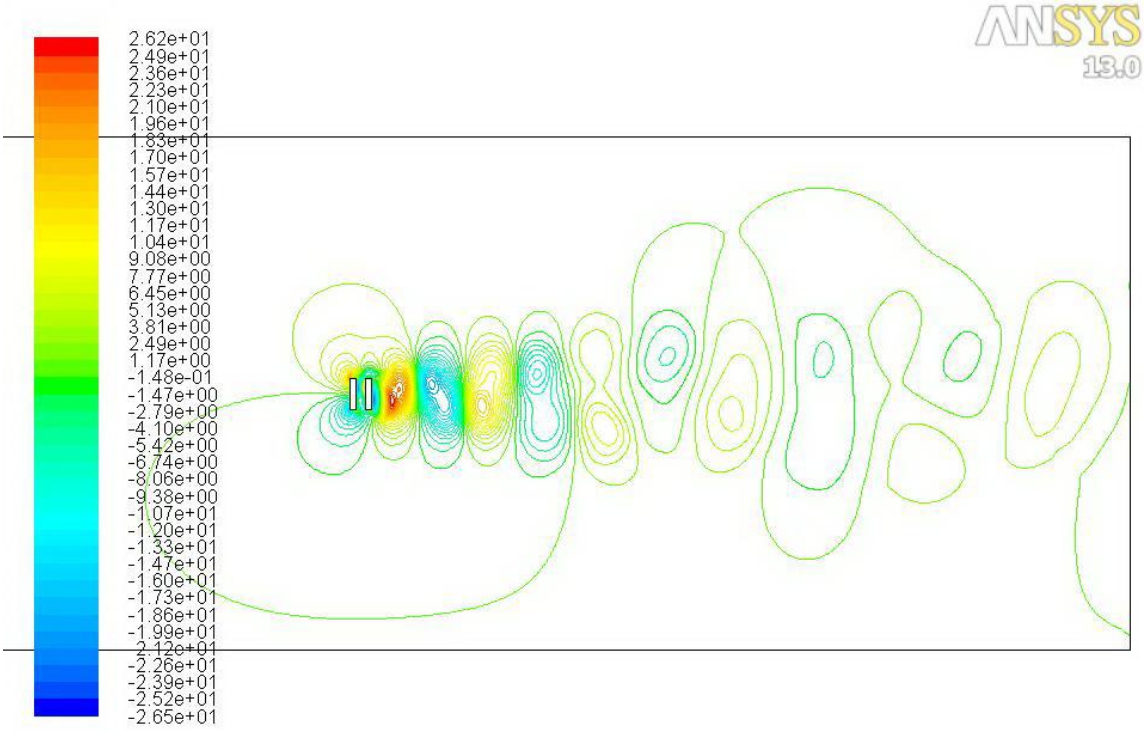

Figure 7. Contours of Y-Velocity ($m\ /\ s$), at $g\ /\ d = 0.3$

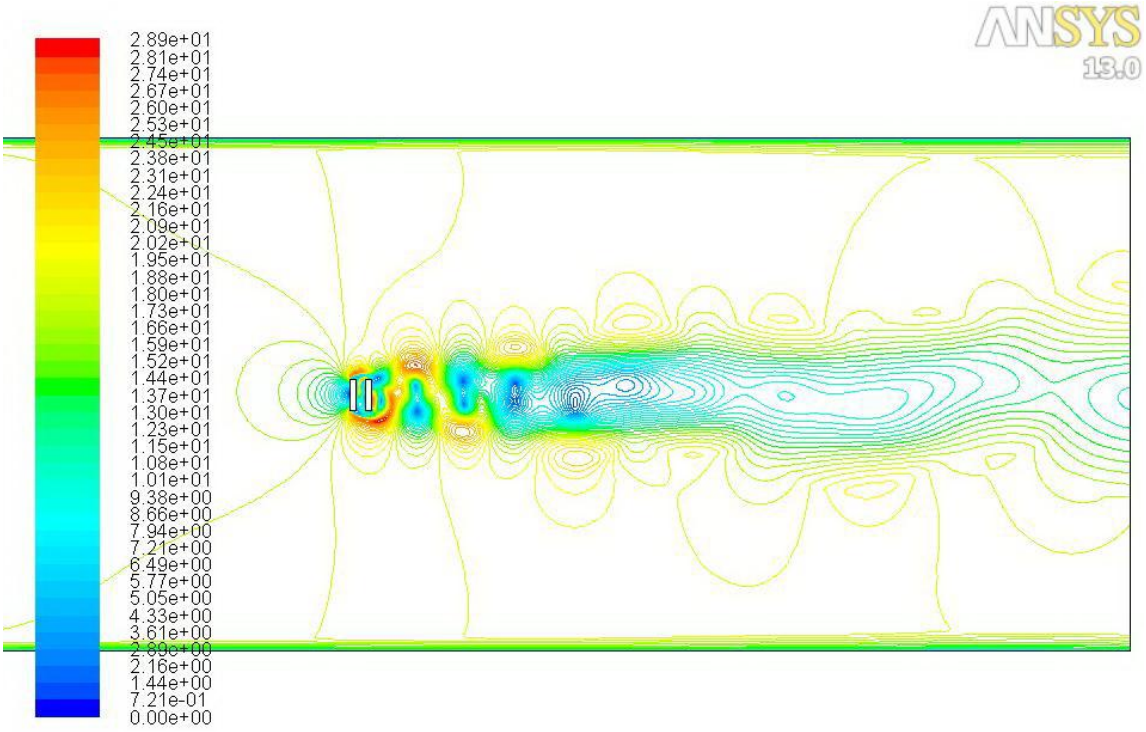

Figure 8. Contours of Velocity Magnitude ($m\ /\ s$), at $g\ /\ d = 0.3$

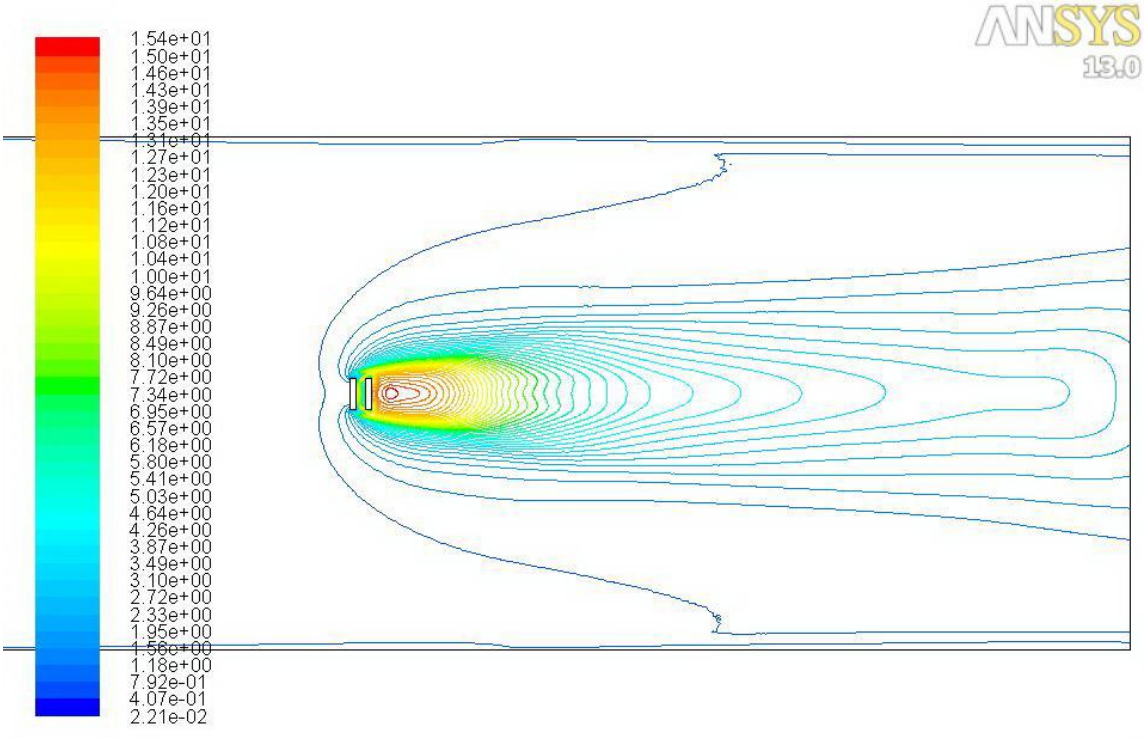

Figure 9. Contours of RMS Velocity Magnitude ($m\ /\ s$), at $g\ /\ d = 0.3$

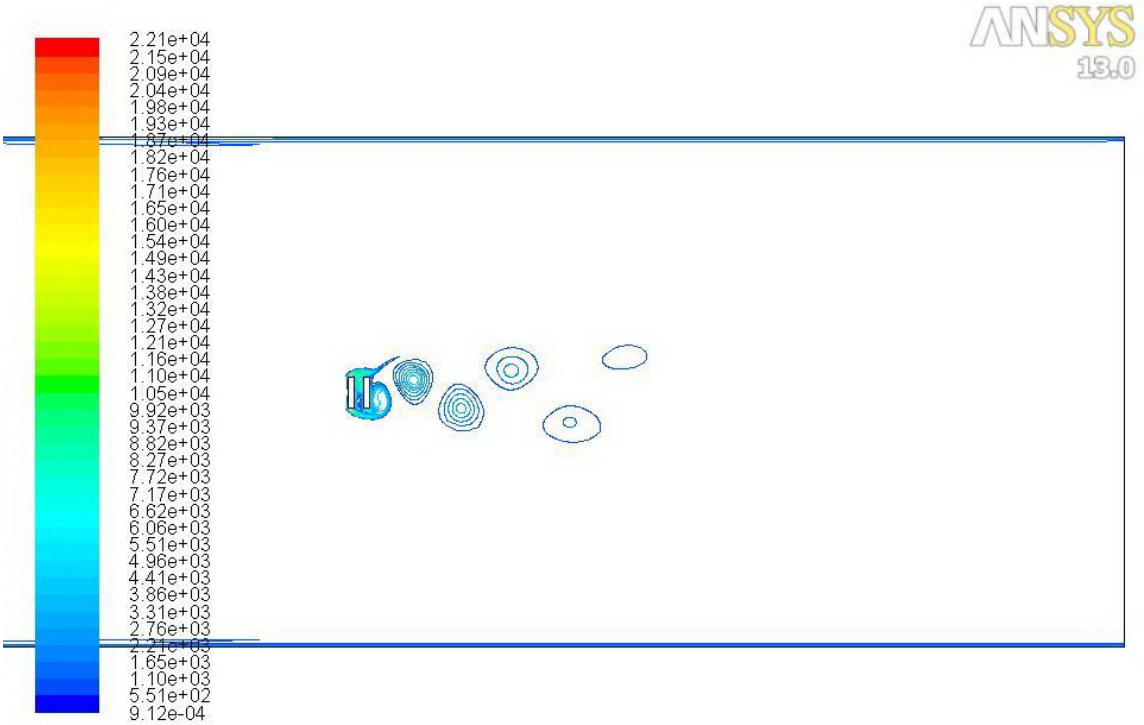

Figure 10. Contours of Vorticity Magnitude $(1\ /\ s)$, at $g\ /\ d = 0.3$

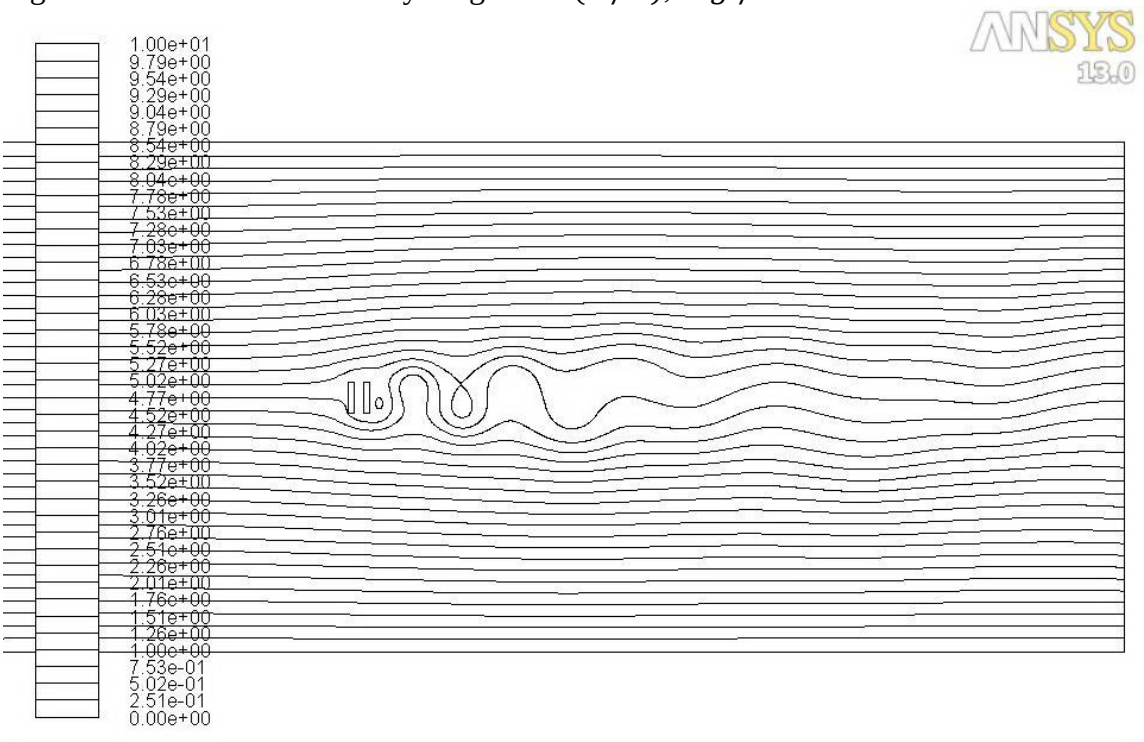

Figure 11. Contours of Stream Function $(kg\ /\ s)$, at $g\ /\ d = 0.3$

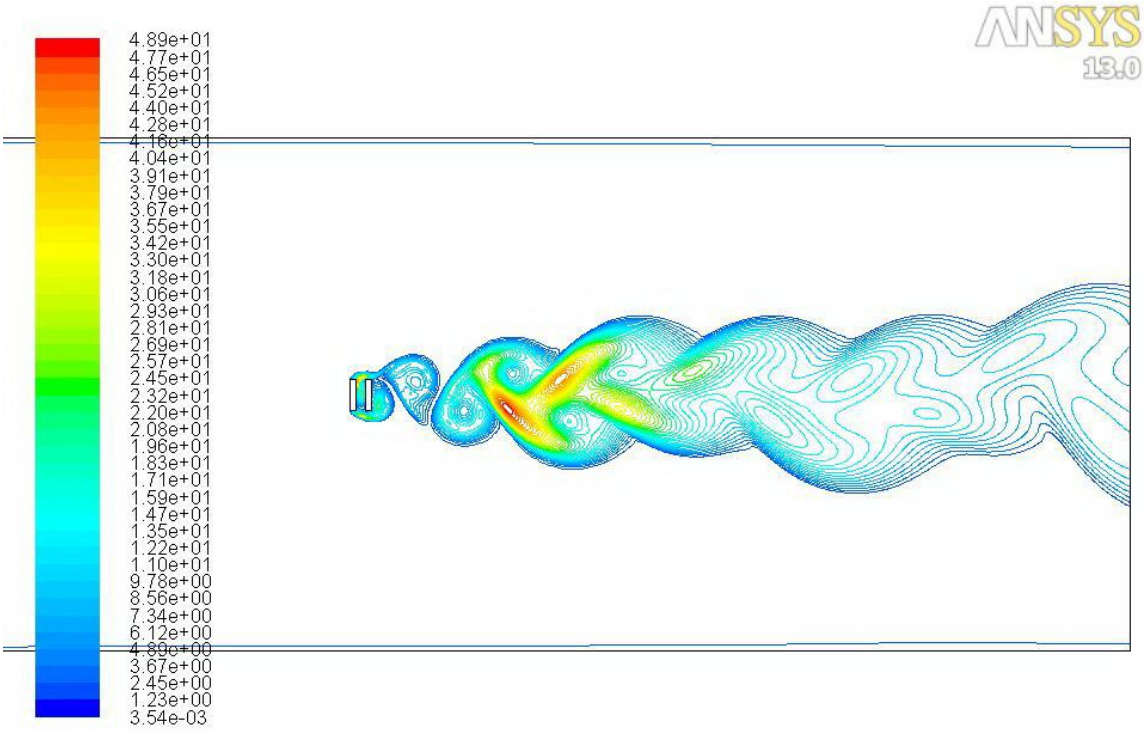

Figure 12. Contours of Turbulent Kinetic Energy (k) (m^2/s^2), at $g\ /\ d = 0.3$

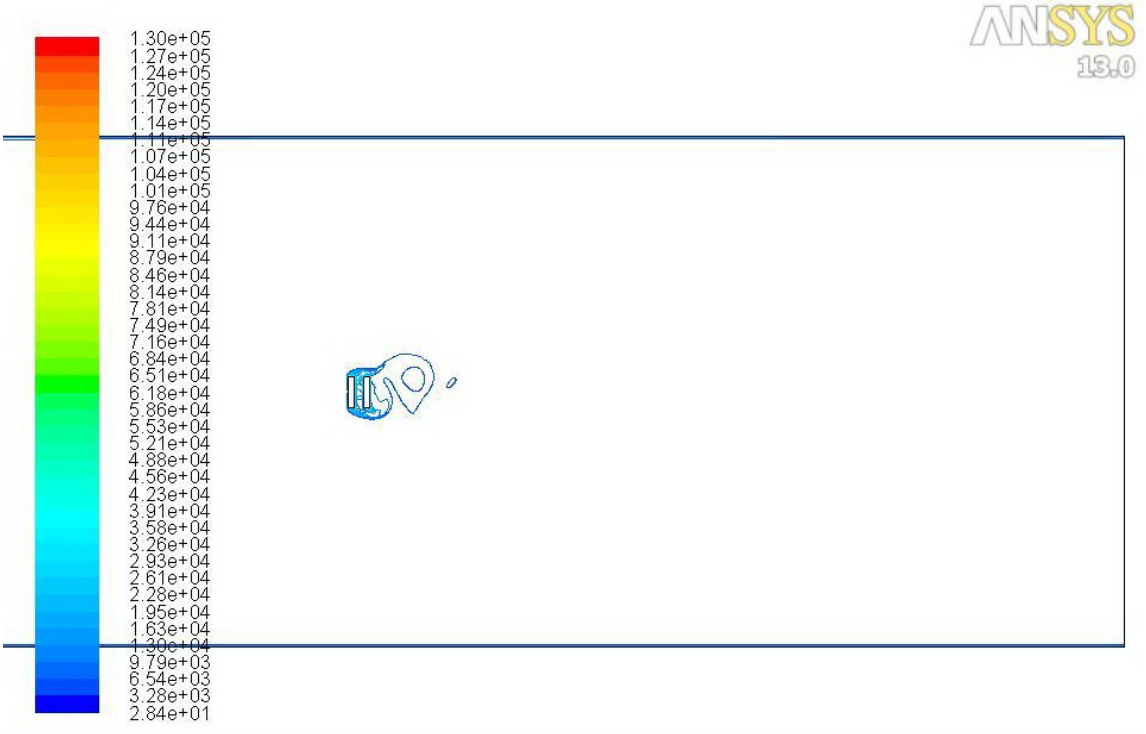

Figure 13. Contours of Specific Dissipation Rate ω ($1\ /\ s$), at $g\ /\ d = 0.3$

For the other cases these graphical outputs consisting of x-velocity contours, stream function contours and vorticity contours are presented in sequence:

X-Velocity contours:

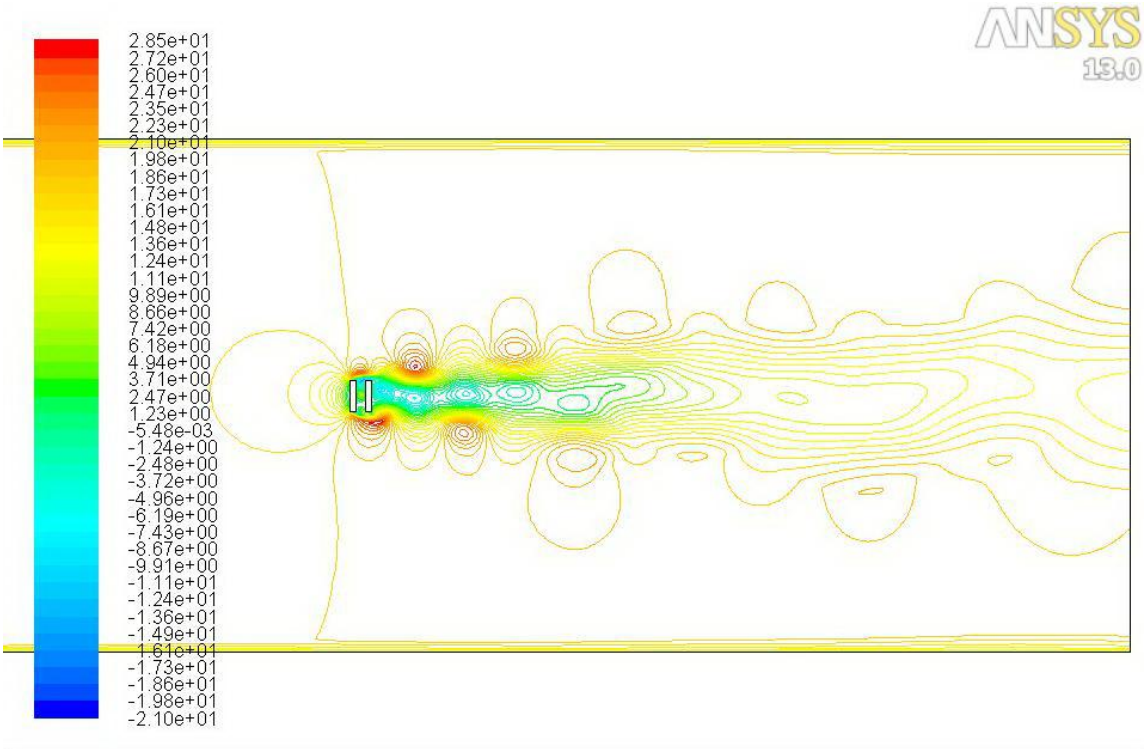

Figure 14. Contours of X-Velocity ($m\ /\ s$), at $g\ /\ d = 0.3$

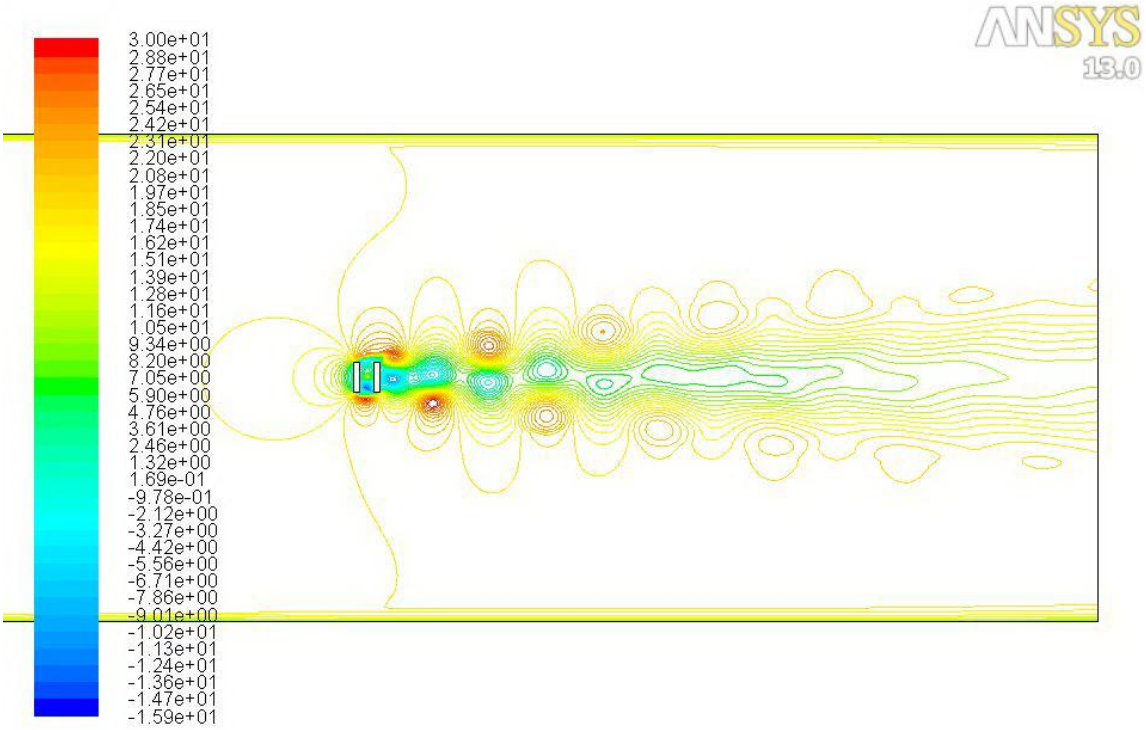

Figure 15. Contours of X-Velocity ($m\ /\ s$), at $g\ /\ d = 0.5$

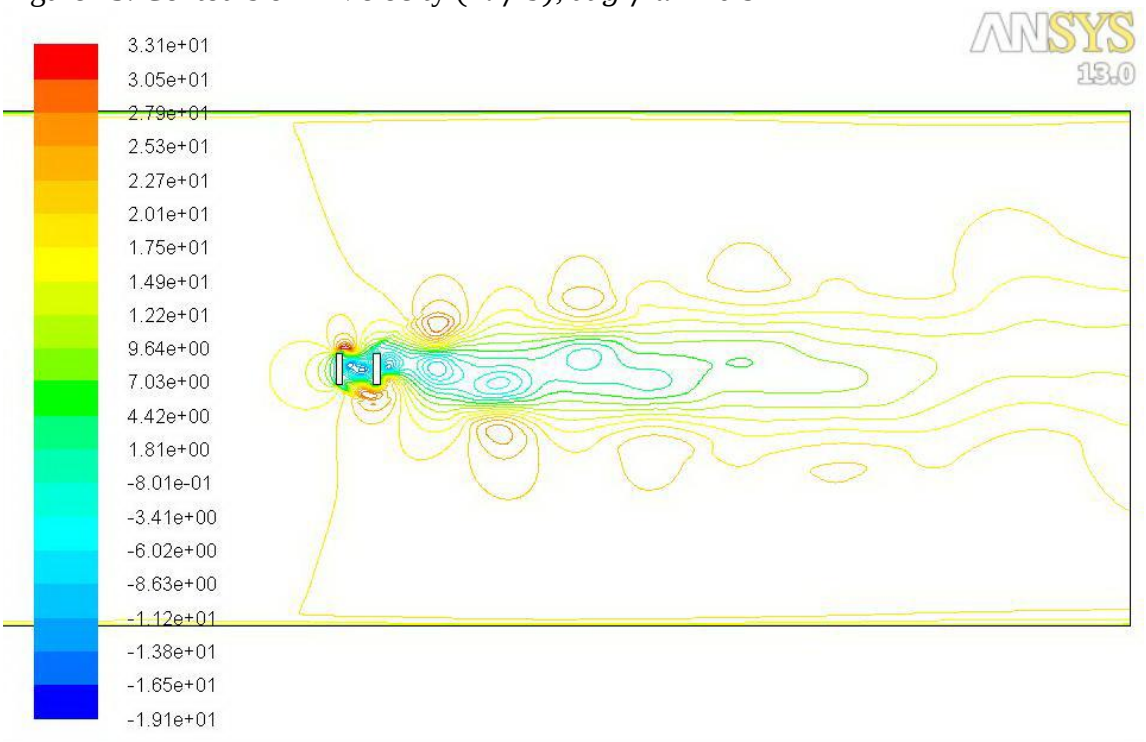

Figure 16.Contours of X-Velocity ($m\ /\ s$), at $g\ /\ d = 1.0$

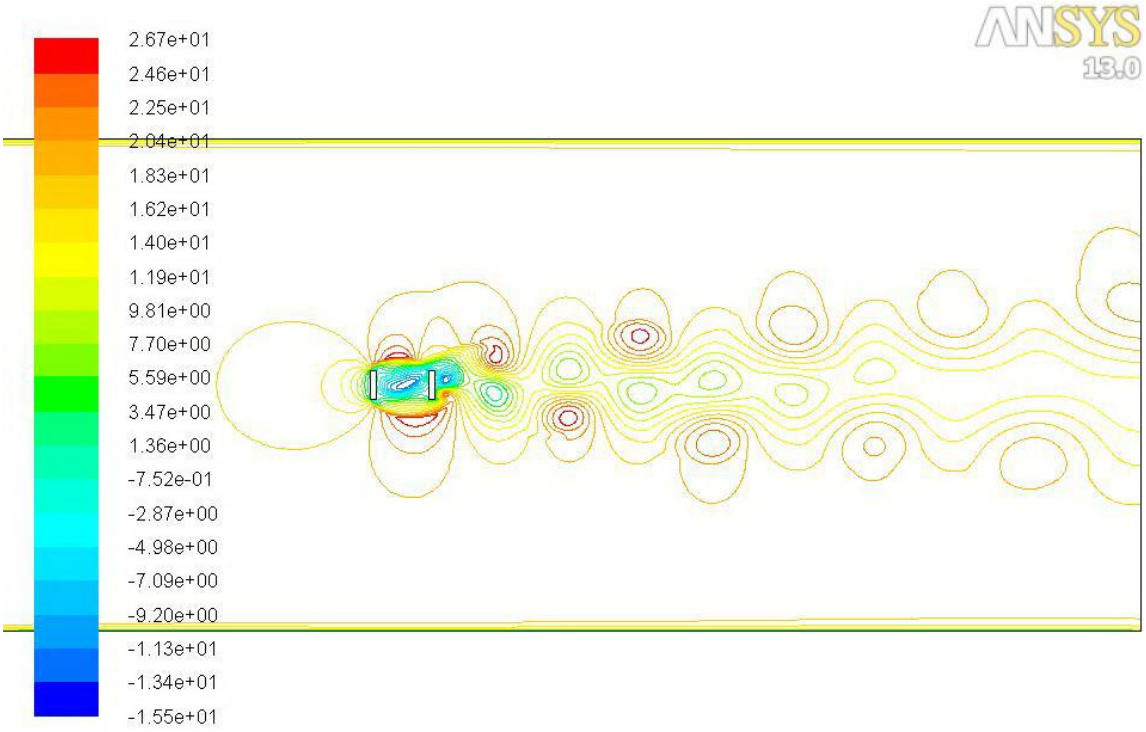

Figure 17. Contours of X-Velocity ($m\ /\ s$), at $g\ /\ d = 1.8$

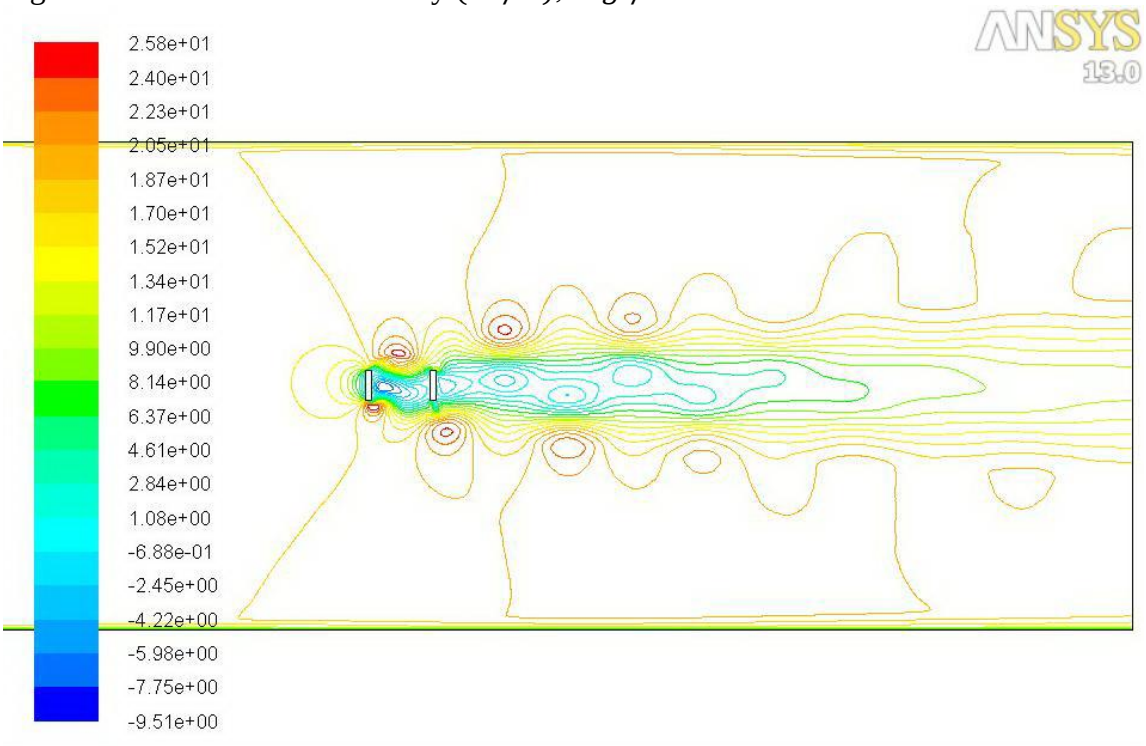

Figure 18. Contours of X-Velocity ($m\ /\ s$), at $g\ /\ d = 2.0$

It should be mentioned that in these cases including gap ratios of 0.5, 1.0 and 2.0 RSM models was employed. The study case of gap ratio 1.0 both $k-\omega\ SST$ and RSM model were employed separately for the analysis and the results were compared by study of x-velocity contour and found to be almost the same for this flow condition.

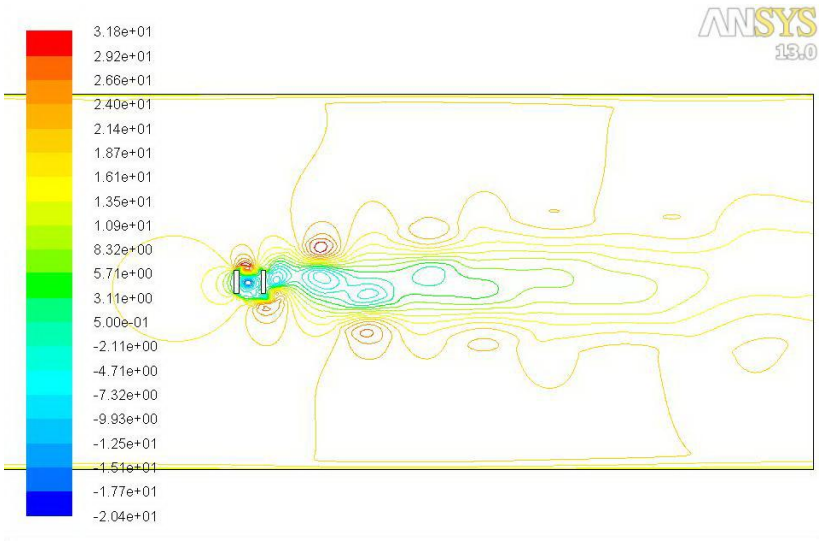

(a)

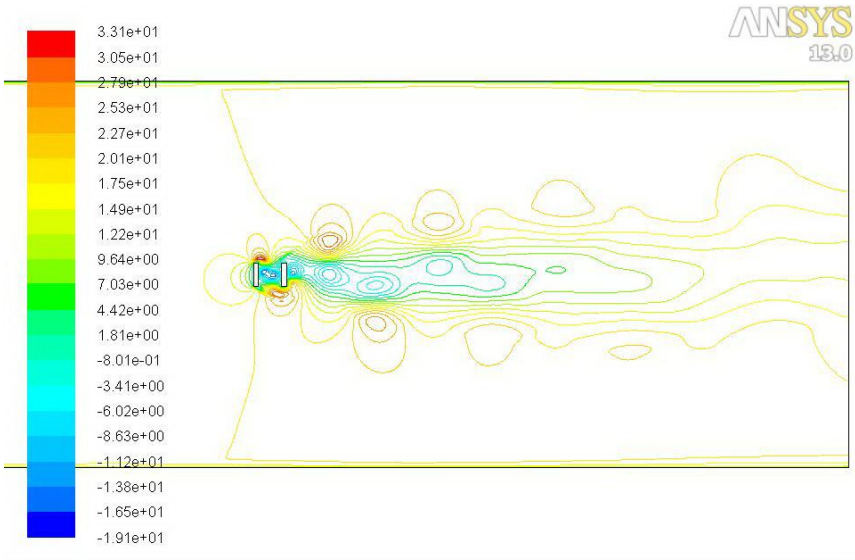

(b)

Figure 19. Contours of X-Velocity $(m\ /\ s)$ at ($g\ /\ d\ =1$), (a) k-ω SST Model and (b) RSM Model

Reynolds stresses $\acute{u}^2, \acute{v}^2$ and $\acute{u}\acute{v}$ are presented at the gap ratios 0.5, 1.0 and 2.0, which are analyzed by the RSM model. This specific model gives these additional stresses that are presented here at the mentioned ratios.

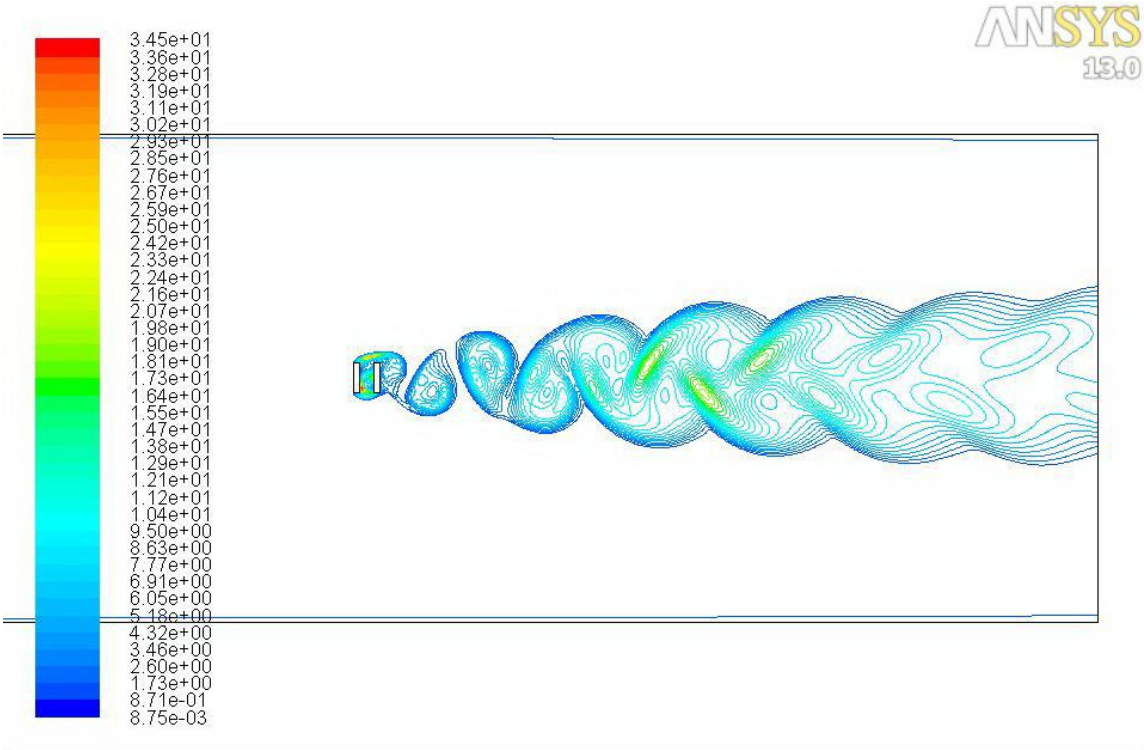

Figure 20. Contours of $\acute{u}'^2$Reynolds Stress (m^2/s^2) at $g\ /\ d = 0.5$

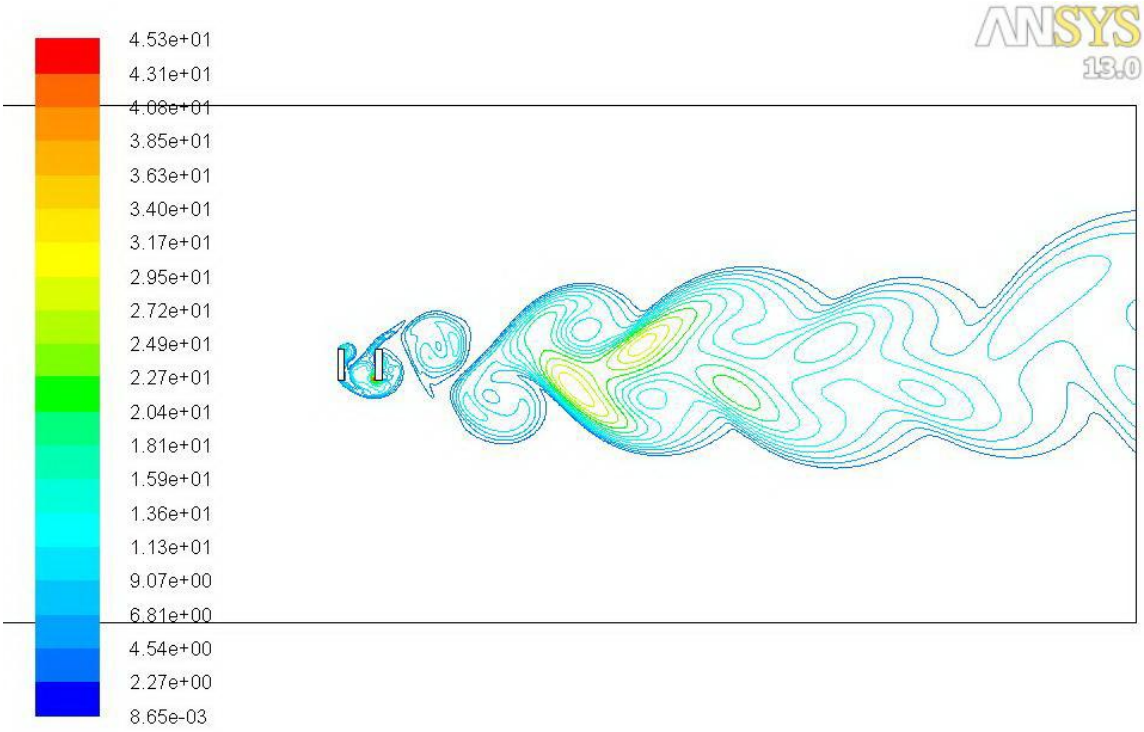

Figure 21. Contours of u'^2 Reynolds Stress (m^2/s^2) at $g\ /\ d = 1.0$

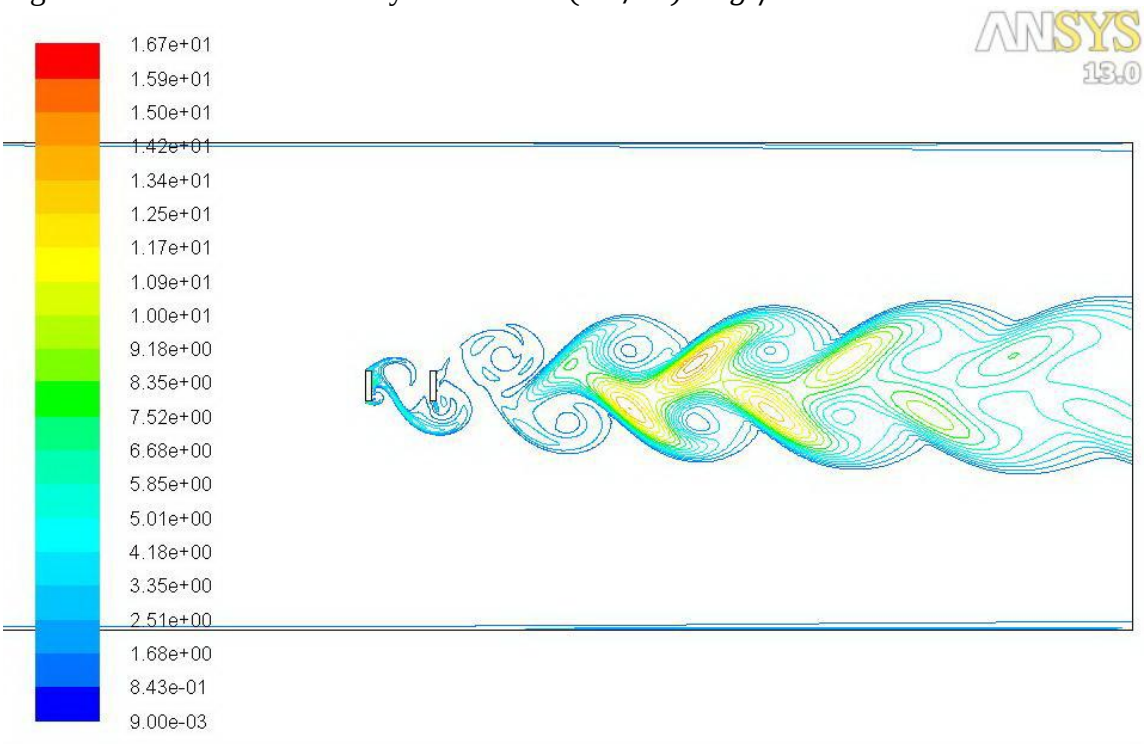

Figure 22. Contours of $\acute{u}'^2$ Reynolds Stress (m^2/s^2) at $g\ /\ d = 2.0$

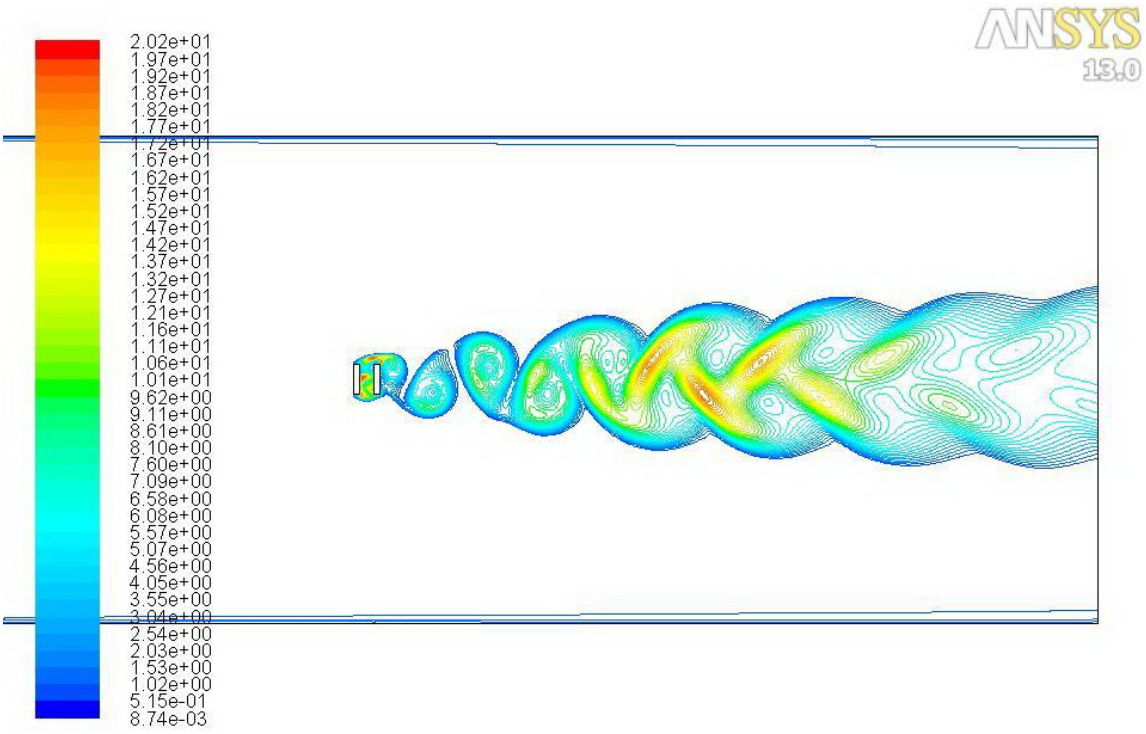

Figure 23. Contours of $\acute{v}'^2$ Reynolds Stress (m^2/s^2) at $g\ /\ d = 0.5$

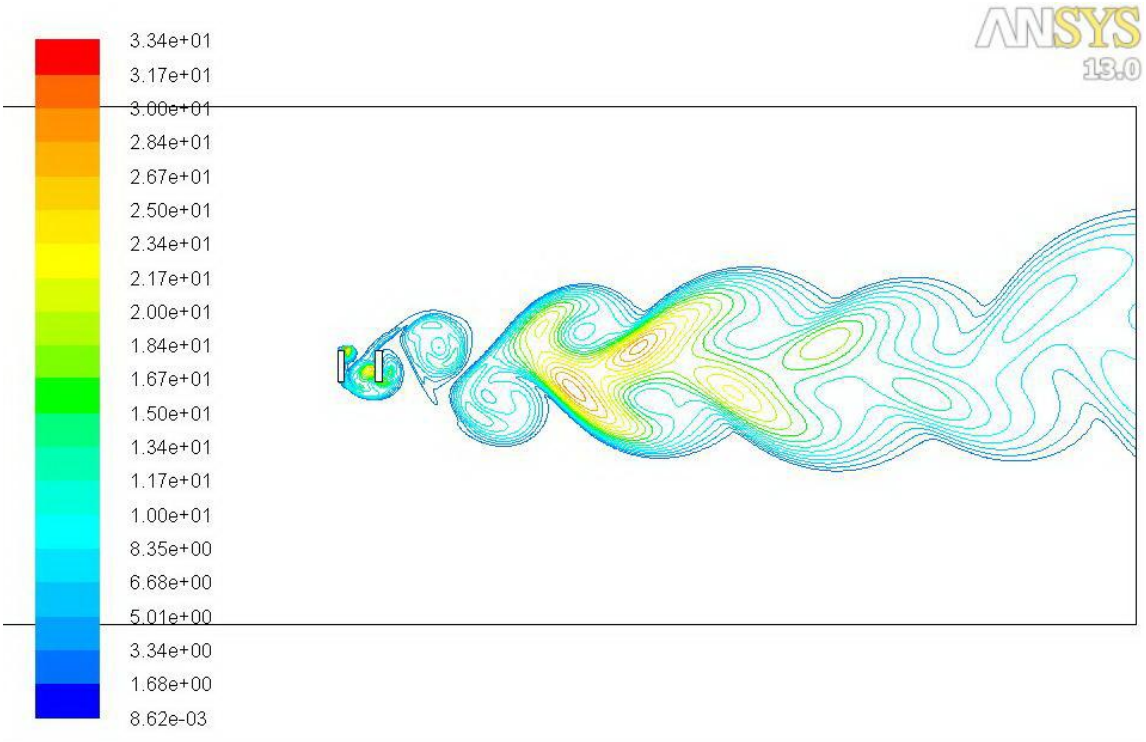

Figure 24. Contours of $\acute{v}'^2$ Reynolds Stress (m^2/s^2) at $g\ /\ d = 1.0$

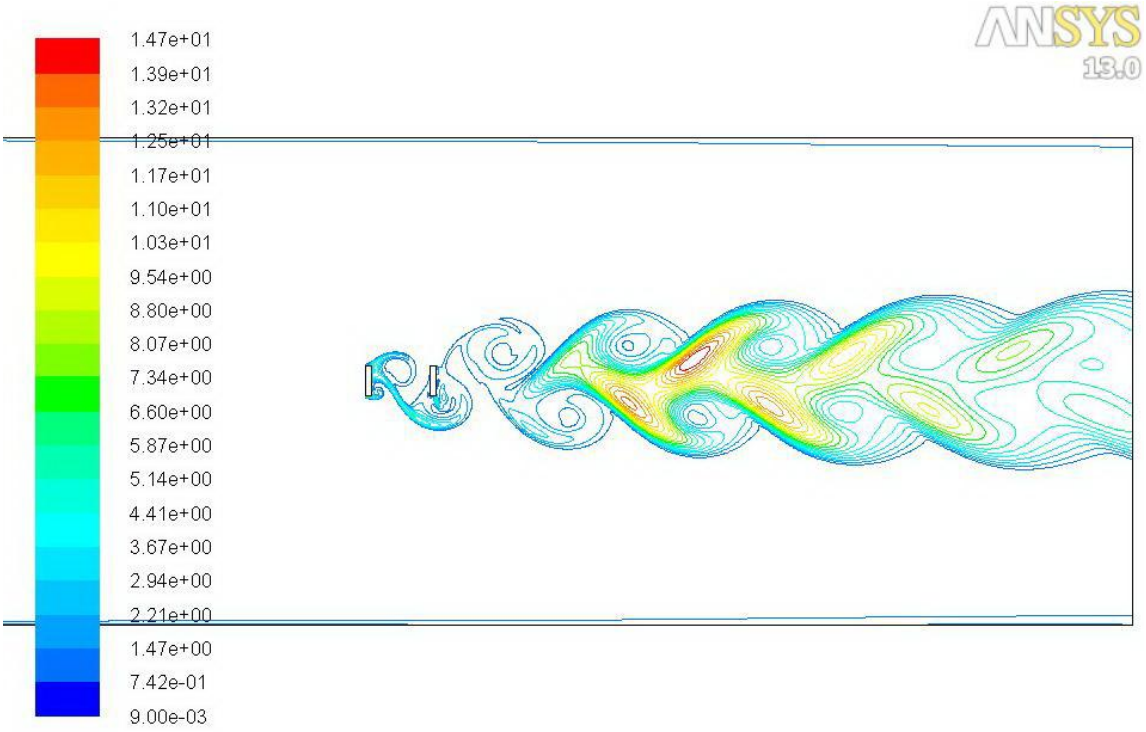

Figure 25.Contours of $\acute{v}'^2$ Reynolds Stress (m^2/s^2) at $g\ /\ d = 2.0$

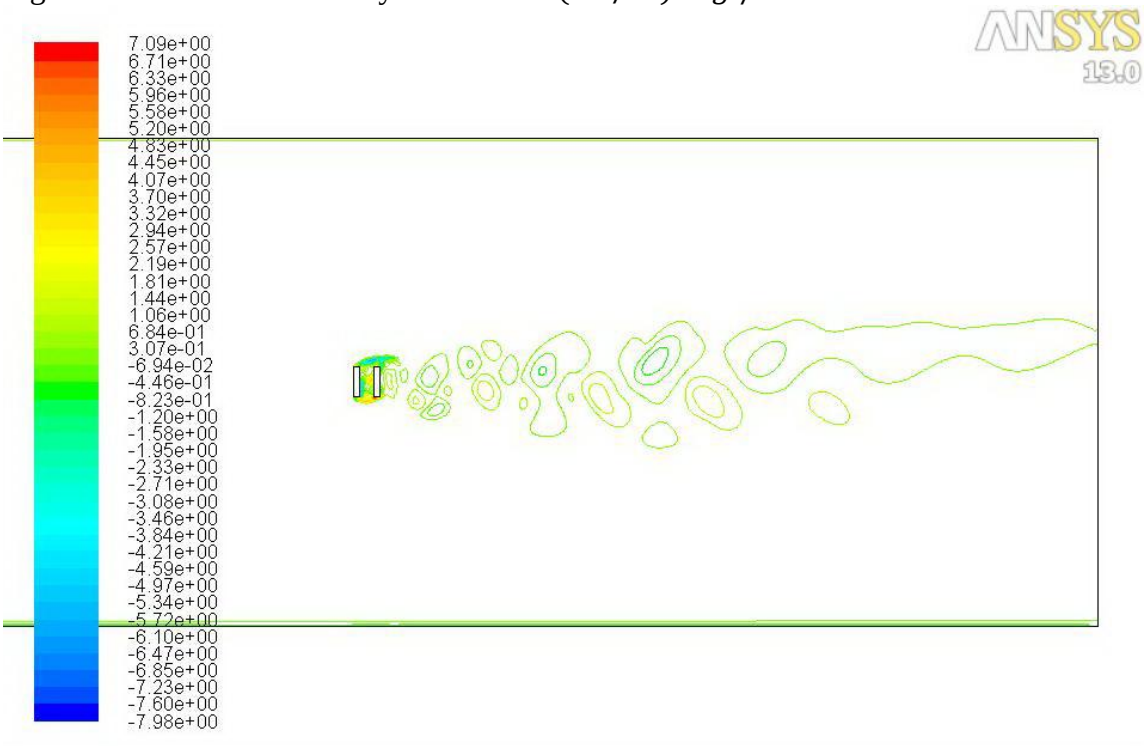

Figure 26. Contours of $\acute{u}\,\acute{v}'$ Reynolds Stress (m^2/s^2) at $g\ /\ d = 0.5$

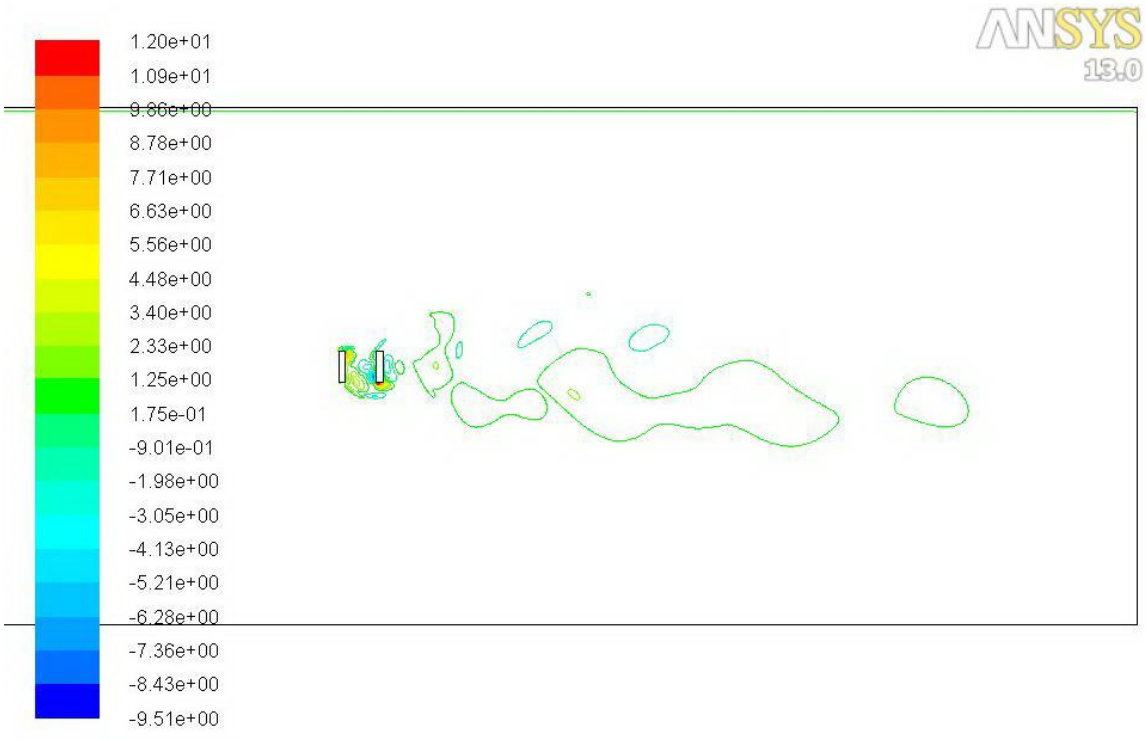

Figure 27. Contours of $\acute{u}\acute{v}$ Reynolds Stress (m^2/s^2) at $g\ /\ d = 1.0$

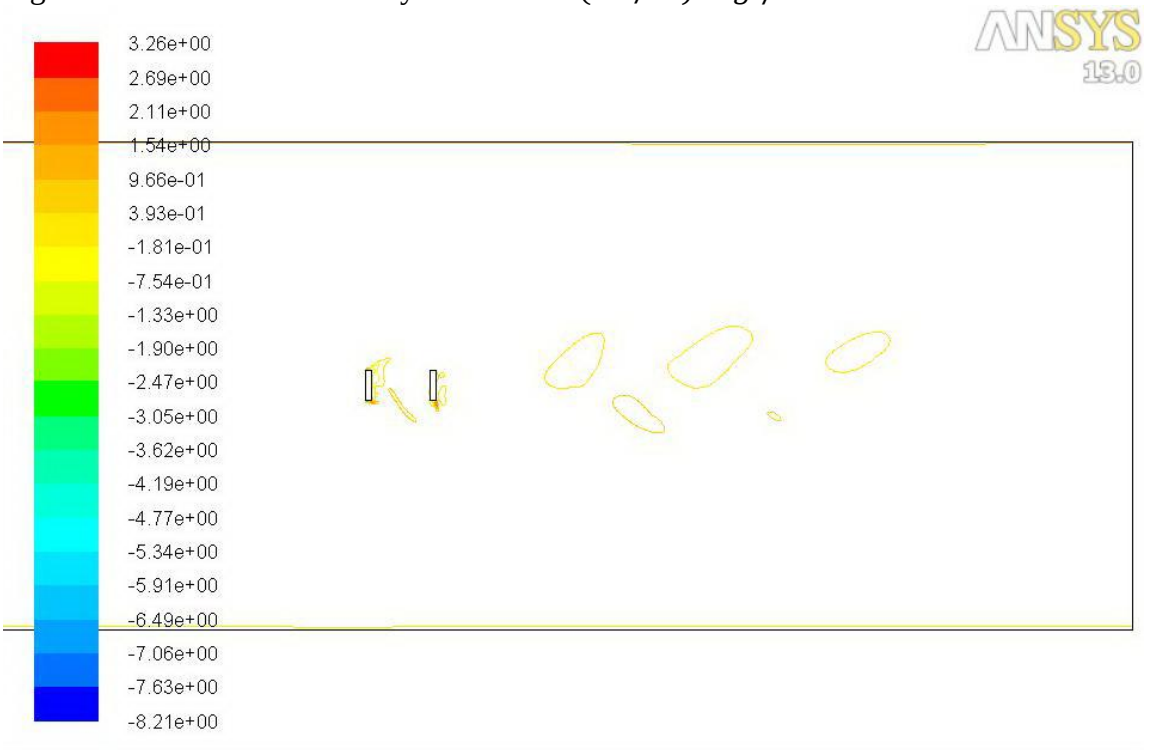

Figure 28. Contours of $\acute{u}\acute{v}$ Reynolds Stress (m^2/s^2) at $g\ /\ d = 2.0$

4.3 Interpretation of Data

Bluff bodies with different gap ratio show different flow behaviour. Difference in smaller gap ratios are negligible. For better understanding of this, similarity a solid body having the overall length equal to the overall length of the gap ratio 0.6 was studied seperately and the x-velocity contours and the vorticity magnitude contours of both cases were compared and found almost similar.

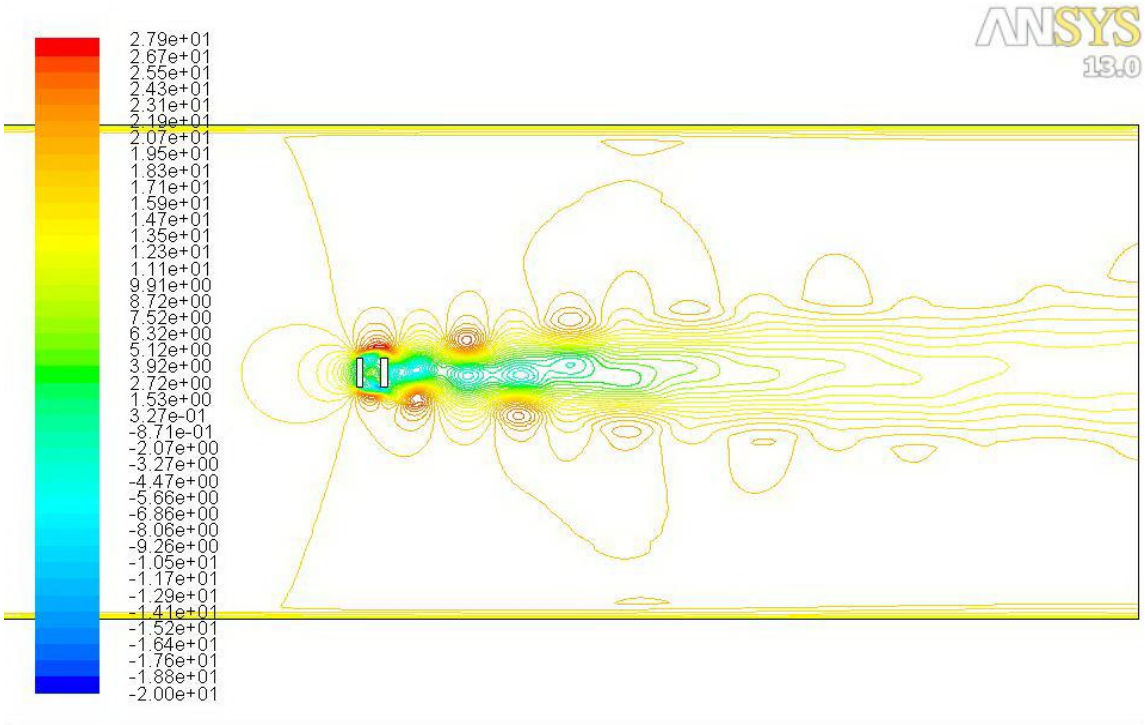

Figure 29. Contours of x-velocity of Tandem Flat Plates $g\ /\ d = 0.6$

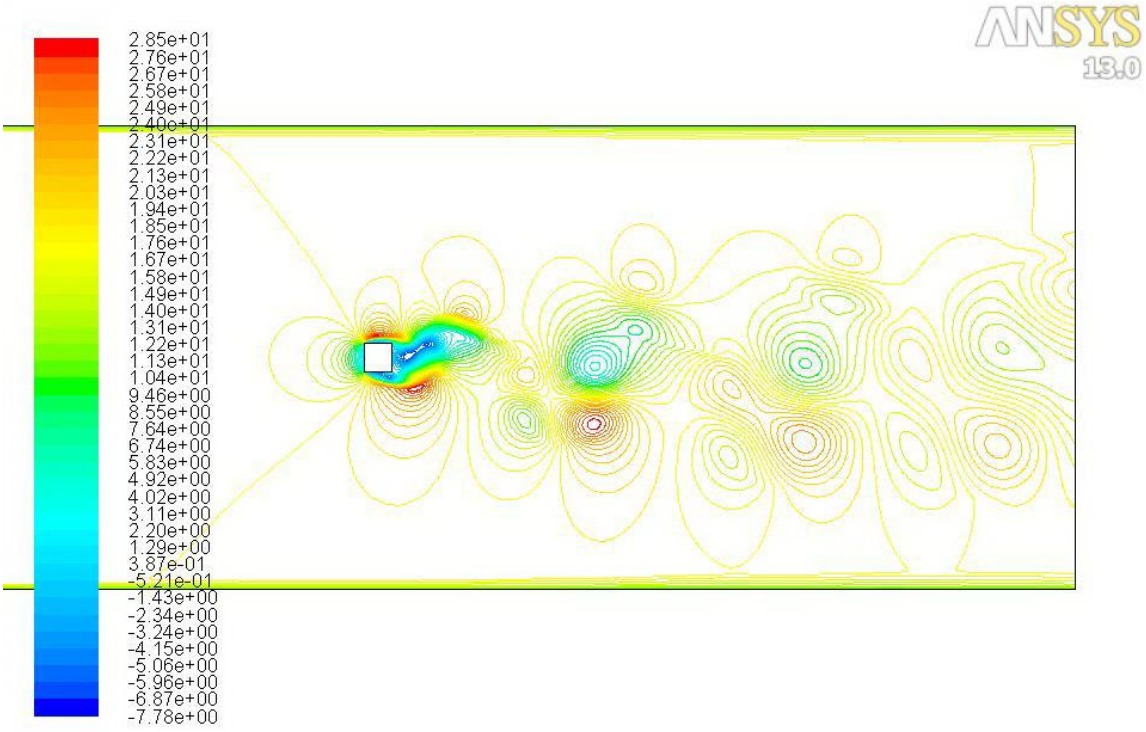

Figure 30. Contours of x-velocity of Square Cylinder

Figure 31. Contours of Vorticity Magnitude at of Tandem Flat Plates $g/d = 0.6$

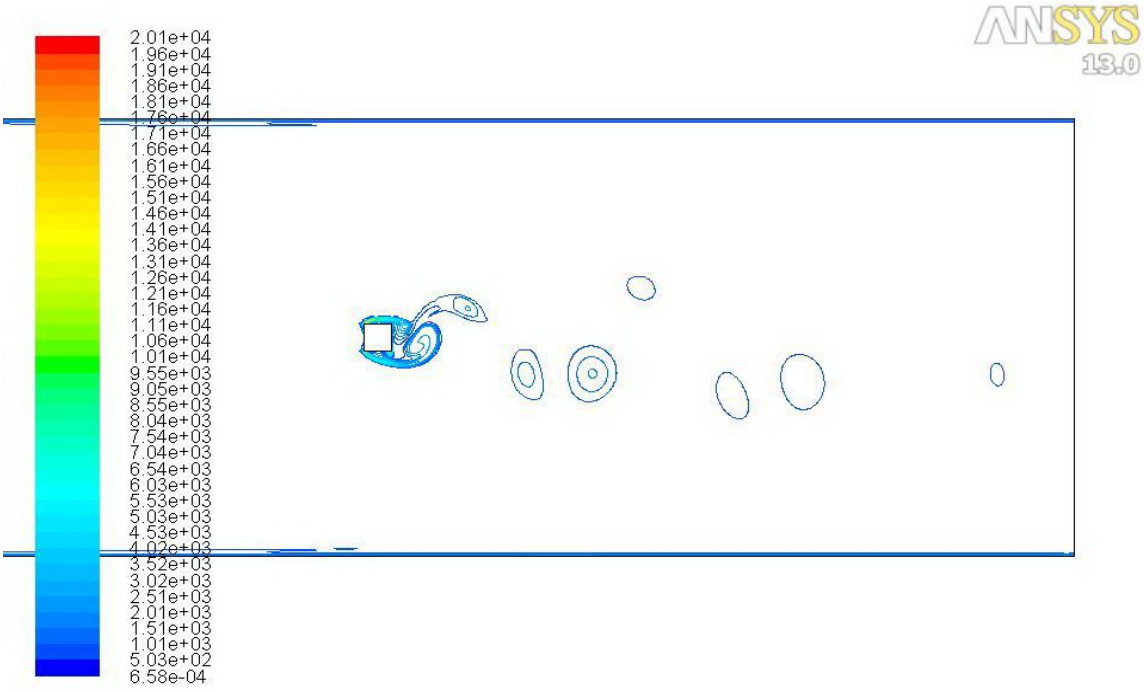

Figure 32. Contours of Vorticity Magnitude of Square Cylinder

As the gap ratio increases the change of flow behaviour between two bodies are distinct. And at large distance there is no interaction of two bodies.

4.4 Comparison of Experimental Data with CFD Results

The available experimental data for the gap ratios of 0.5, 1.0 and 2.0 are as follows [28]:

1. Contours of stream-wise velocity
2. Contours of traverse velocity
3. Incoherent normal stresses in stream-wise direction
4. Incoherent Normal Stresses in Traverse Direction at $x/d = 2$
5. Incoherent Normal Stresses in Traverse Direction at $x/d = 4$
6. Contours of $\acute{u}\acute{v}$ Reynolds stresses

The results of CFD analysis presented before were further processed to be of the same order of experimental data as listed above. This includes normalizing of x-velocity and y-velocity with free stream velocity and Reynolds stresses were normalized with the square of free stream velocity.

These two sets of data are arranged in the following six pages, each page presenting in the first row are the CFD contours and in the second row are the experimental data (figures 33 to 38).

This study shows considerable agreement between CFD and the results of wind tunnel studies and considering the difficulties of the experimental analysis. This is a valuable and promissing outcome for the further developments of the CFD method to solve the relevant engineering problems.

Another sets of experimental data presented in reference [28] are sets of graphs giving the variation of mean x-velocity at different sections of wind tunnel arrangement, pages 94, 95. The same kind of graph is drawn for the case of gap ratio $g/d = 0.6$, figure 39.

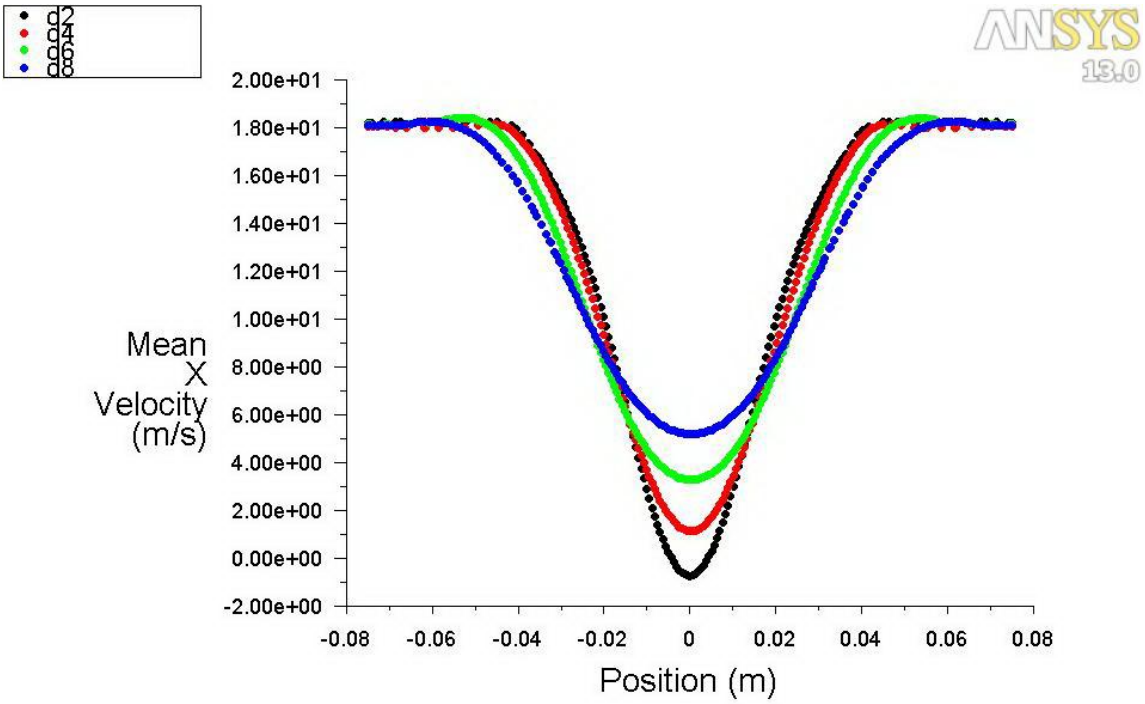

Figure 39. Mean X Velocity $at\ g/d = 0.6$

This graph is also is similar to the experimental graphs.

Chapter 5

CONCLUSIONS

5.1 Summary

Nowadays, computational fluid dynamics are widely used to simulate complex flows in many engineering fields. Their capabilities caused the presence of many workshops that are trying to solve the problems associated with this new technology. They check the validity and applicability of different methods of CFD in different areas.

The aim of this study was to evaluate the capability of CFD analysis in the prediction of the flow behavior around the engineering structures and insulations and this was carried out by the use of the existing wind tunnel investigation results, therefore the same problems were analyzed by the CFD method and the resulting data were compared by the experimental data. And the close agreement between two sets of data proved that the CFD method regarding the limitation and the expense of wind tunnel model studies of flow behavior and could be developed and applied to the more complicated problems.

5.2 Future Study

According to the fact that the flow has three dimensional property and the triple decomposition techniques give more realistic results as the coherent property of the velocity is also accounted, the three dimensional study of this case recommended.

REFERENCES

[1] Fujii, K. (2005). Progress and future prospects of CFD in aerospace - Wind tunnel and beyond. *Progress in Aerospace Sciences*, 41 (6), 455-470.

[2] Billah, K. and Scanlan, R. (1991). Resonance, Tacoma Narrows Bridge Failure, and Undergraduate Physics Textbooks. *American Journal of Physics*, 59 (2), 118-124

[3] Fujii, K. (2009, September 23). Realization of prof. kuwahara'smessages - after almost 30 years' effort in CFD - [Web log message]. Retrieved from http://accc.riken.jp/assets/nobeyama/1-2Fujii.pdf

[4] Cengel, A. and CIMBALA, M. (2006). *Fluid mechanics fundamentals and applications*. (p. 570). New York: McGraw-Hill.

[5] Wu, J. and Hu, Y. (1995). A numerical study of wake interference behind two side-by-side and tandem circular cylinders. *Journal of the Chinese Society of Mechanical Engineers*, *16* (2), 109-122.

[6] Bearman, P.W. (1965). Investigation of the flow behind a two-dimensional model with a blunt trailing edge and fitted with splitter plates. *Journal of Fluid Mechanics*, 21, 241-255.

[7] Bearman, P.W. and Trueman, D.M. (1972). Investigation of flow around rectangular cylinders. *AERONAUT QUART*, 23, 229-237.

[8] Auteri F., Belan M., Gibertini G. aand Grassi D. (2008). Normal flat plates in tandem: An experimental investigation. *Journal of Wind Engineering and Industrial Aerodynamics*, 96 (6-7), 872-879.

[9] Liu C. H. and Chen J. M. (2002).Observations of hysteresis in flow around two square cylinders in a tandem arrangement. *Journal of Wind Engineering and Industrial Aerodynamics*, 90 (9), 1019-1050.

[10] Yen S.C., San K.C. and Chuang T.H. (2008). Interactions of tandem square cylinders at low Reynolds numbers. *Experimental Thermal and Fluid Science*, 32 (4), 927-938.

[11] Xu, G. and Zhou, Y. (2004). Strouhal numbers in the wake of two inline cylinders. *Experiments in Fluids*, *37*, 248-256.

[12] Wei C.Y., Chang J.R. (2002). Wake and base-bleed flow downstream of bluff bodies with different geometry. *Experimental Thermal and Fluid Science*, 26 (1), 39-52.

[13] Mazharoglu C. and Hacisevki H. (1999). Coherent and incoherent flow structures behind a normal flat plate. *Experimental Thermal and Fluid Science*, 19 (3), 160-167.

[14] Hacisevki, H. and Mazharoglu, C. Triple decomposition technique applied for near wake flow measurement. 272-275.

[15] Kiya, M., Matsumara, M. (1988). Incoherent turbulence structure in the near wake of a normal plate. *Journal of Fluid Mechanics*, 190, 343-356.

[16] Auteri F., Belan M., Gibertini G. and Grassi D. (2008). Normal flat plates in tandem: An experimental investigation. *Journal of Wind Engineering and Industrial Aerodynamics*, 96 (6-7), 872-879.

[17] Bosch, G. and Rodi, W. (1996). Simulation of vortex shedding past a square cylinder near a wall. *International Journal of Heat and Fluid Flow*, *17*(3), 267-275.

[18] Edamoto, K. and Kawahara, M. (1998). Finite element analysis of two- and three-dimensional flows around square columns in tandem arrangement. *International Journal for Numerical Methods in Fluids*, 28, 95–112.

[19] Ishigai, S. and Nishimura, X., Cho, X. (1972). Experimental study on structure of gas flow in tube banks with axis normal to the flow. *Bull. JSME*, 15, 949-956.

[20] Zdravkovich, M. M. (1987). The effects of interference between circular cylinders in cross flow. *Journal of Fluids and Structures*, 239-261.

[21] Bearman, P. W. and Wadcock, A. J. (1973). The interference between a pair of circular cylinders normal to a stream. *Journal of Fluid Mechanics*, 61, 499-511.

[22] Chen L., Tu J.Y. and Yeoh G.H. (2003). Numerical simulation of turbulent wake flows behind two side-by-side cylinders. *Journal of Fluids and Structures*, 18 (3-4), 387-403.

[23] Mansour, N. N., Kim, J. and Moin, P. (1989). Near-wall $k-\varepsilon$ turbulence modeling. *Journal of AIAA*, 27 (8), 1068-1073.

[24] Tamaddon-Jahromi H.R., Townsend P. and Webster M.F. (1994). Unsteady viscous flow past a flat plate orthogonal to the flow. *Computers and Fluids*, 23 (2), 433-446.

[25] Joshi, D. S., Vanka, S. P. and Tafti, D. K. (1994). Large eddy simulation of the wake of a normal flat plate. *Boundary Layer and Free Shear Flows ASME, 184*, 231-242.

[26] N Meroney, R., Leitl, B. M., Rafailidis, S. and Schatzmann, M. (1999). Wind-tunnel and numerical modeling of flow and dispersion about several

building shapes. *Journal of Wind Engineering and Industrial Aerodynamics*, *81*(1-3), 333-345.

[27] Skye H.M., Nellis G.F. and Klein S.A. (2006). Comparison of CFD analysis to empirical data in a commercial vortex tube. *International Journal of Refrigeration*, 29 (1), 71-80.

[28] Hacisevki, H. (2001). Vortex shedding in tandem arrangement. 23-29, 70-90.

[29] Jha, Vineetkumar. (2008, October). *Carbon black filler reinforcement of elastomers*. Retrieved from http://www.sems.qmul.ac.uk/research/honours/doc.php?id=33

[30] Holmes, J. D. (2001). *Wind loading of structures*. (First ed., pp. 157-158). London: Spon Press.

[31] Versteeg, H. K. and Malalasekera, W(2007). *An introduction to computational fluid dynamics: the finite volume method*. (2 ed.). Newjersey: Prentice Hall.

[32] Technical Writer (Fluid Mechanics Instrument Division), (1996). *Model 1500 series flowpoint velocity measuring system:instruction manual*. (pp. 1-1-1-3). St. Paul: TSI Incorporated.

[33] Sezai, I. (2009). How does a cfd code work? [Web log message]. Retrieved from http://me.emu.edu.tr/sezai/ME555/Chapter%201.pdf

[34] Owen, S. (2005). Geometry modeling & grid generation [Web log message]. Retrieved from http://www.stanford.edu/class/me469b/handouts/geoandgrid.pdf

[35] Fluent Inc. (2006, October 12). *Fluent 6.3 getting started guide*. Retrieved from http://my.fit.edu/itresources/manuals/fluent6.3/help/html/gs/main_pre.htm

APPENDICES

Appendix A: Wind Tunnel Experiment

An open type subsonic wind tunnel, 10 meters long with a working section $0.5\,m \times 0.5\,m$ and $1.4m$ long was used. Contraction ratio of the tunnel is $10:1$ and at the entrance a $1.6\,m \times 1.6\,m$ triangular sectioned flow straightener sandwiched with two layers of wire mesh was installed and calibrated. The tunnel has a free stream turbulence level of about $0.5 - 0.8\%$ at the top speed of $30\,m/s$. The velocity measuring system of this wind tunnel is a fully-integrated, thermal anemometer-based system which measures mean and fluctuating velocity components in air [32]. The tunnel speed adjustable through a 12 kW frequency controlled speed. The free stream velocity of air kept constant at $16.4 \pm 2\%$ for this specified experiment. As the vortex shedder, a flat plate made of plexiglass of dimensions 30 mm width; 500 mm height and 6 mm thickness were used. The Reynolds number was 33000 [13].

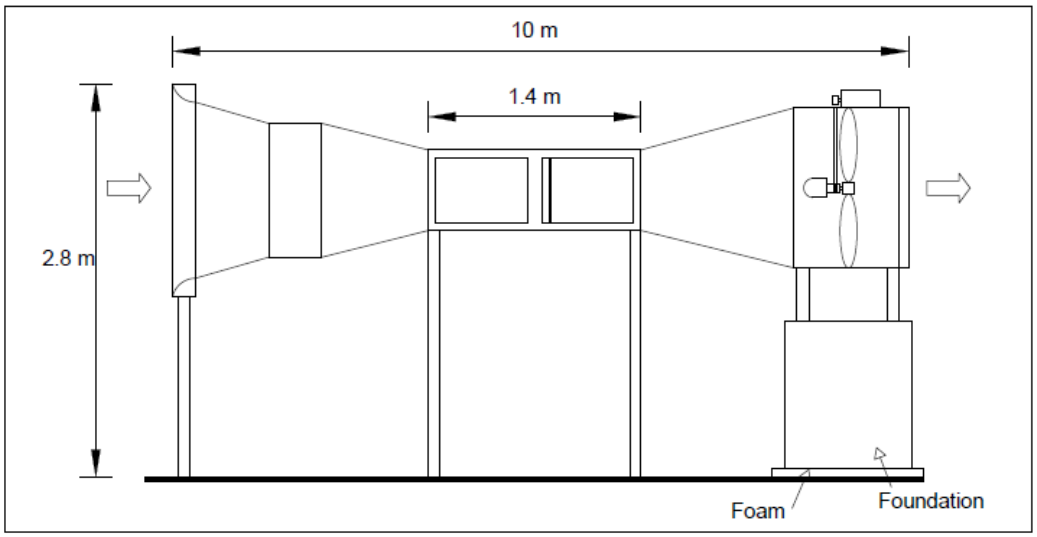

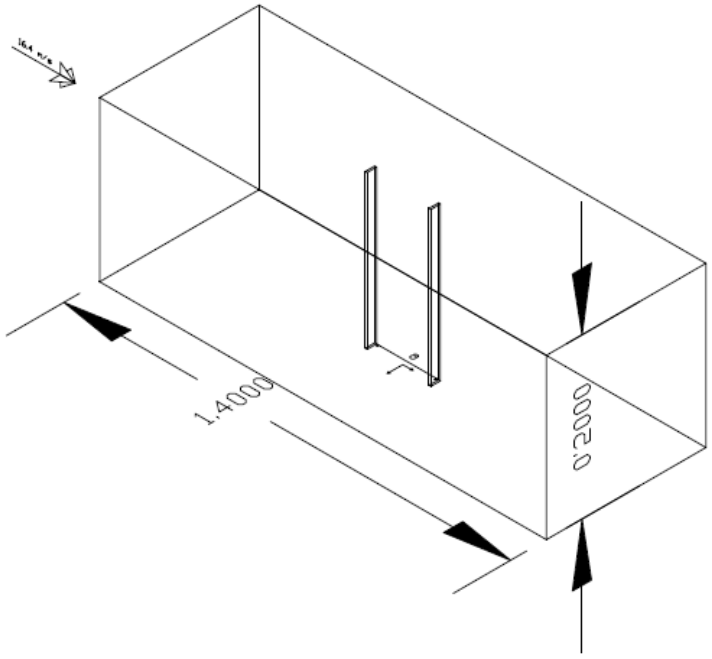

Figure 40. Schematic View of Wind Tunnel and Test Section with Loaded Plates

Appendix D: Turbulence Modeling

D.1 Shear-Stress Transport (SST) $k-\omega$ Model

D.1.1 Transport Equations for the $SST\ k-\omega$ Model

The turbulence kinetic energy, k and the specific dissipation rate, ω is obtained from the following transport equations:

$$\frac{\partial}{\partial t}(\rho k)+\frac{\partial}{\partial x_i}(\rho k u_i)=\frac{\partial}{\partial x_j}\left(\Gamma_k \frac{\partial k}{\partial x_j}\right)+\widetilde{G_k}-Y_k+S_k \quad \text{(D-1)}$$

and

$$\frac{\partial}{\partial t}(\rho \omega)+\frac{\partial}{\partial x_i}(\rho \omega u_i)=\frac{\partial}{\partial x_j}\left(\Gamma_\omega \frac{\partial \omega}{\partial xi}\right)+G_\omega-Y\omega+D\omega+S\omega \quad \text{(D-2)}$$

Where,

$\widetilde{G_k}$, is the generation of turbulence kinetic energy due to mean velocity gradients,

G_ω, represents the generation of ω,

$\Gamma_k\ and\ \Gamma_\omega$, represent the effective diffusivity of k and ω,

Y_k, represent the dissipation of k and ω due to turbulence and

$S_k\ and\ S_\omega$, are user-defined source term.

D.1.2 Modeling the Effective Diffusivity

The effective diffusivities for the $SST\ k-\omega$model are given by

$$\Gamma_K = \mu + \frac{\mu_t}{\sigma_k} \tag{D-3}$$

$$\Gamma_\omega = \mu + \frac{\mu_t}{\sigma_\omega} \tag{D-4}$$

Where σ_k and σ_ω are the turbulence Prandtl numbers for k and ω, respectively. The turbulent viscosity,μ_t is computed as follows:

$$\mu_t = \frac{\rho k}{\omega} \frac{1}{max\left[\frac{1}{\alpha^*}, \frac{SF_2}{a_1 \omega}\right]} \tag{D-5}$$

Where S is the strain rate magnitude and

$$\sigma_k = \frac{1}{F_1/\sigma_{k,1} + (1-F_1)/\sigma_{k,2}} \tag{D-6}$$

$$\sigma_\omega = \frac{1}{F_1/\sigma_{\omega,1} + (1-F_1)/\sigma_{\omega,2}} \tag{D-7}$$

The coefficient α^* damps the turbulent viscosity causing a low-Reynolds number correction.

F_1 And F_2 are given by

$$F_1 = \tanh(\phi_1^4) \tag{D-8}$$

$$\phi_1 = min\left[max\left(\frac{\sqrt{k}}{0.09\omega y}, \frac{500\mu}{\rho y^2 \omega}\right), \frac{4\rho k}{\sigma_{\omega,2} D_\omega + y^2}\right] \tag{D-9}$$

$$D_\omega^+ = max\left[2\rho \frac{1}{\sigma_{\varpi,2}} \frac{1}{\varpi} \frac{\partial k}{\partial x_i} \frac{\partial \omega}{\partial x_i}, 10^{-10}\right] \tag{D-10}$$

$$F_2 = tanh(\phi_2^2) \tag{D-11}$$

$$\phi_2 = max\left[2\frac{\sqrt{k}}{0.09\omega y}, \frac{500\mu}{\rho y^2 \omega}\right] \quad \text{(D-12)}$$

Where, y is the distance to the next surface and D_ω^+ is the positive portion of the cross-diffusion term.

D.1.3 Modeling Turbulence Production

D.1.3.1 Production of k

The term $\tilde{G}_k$ represents the production of turbulence kinetic energy, and is defined as:

$$\tilde{G}_k = \min(G_k, 10\rho\beta^* k\omega) \quad \text{(D-13)}$$

D.1.3.2 Production of ω

The term G_ω represents the production of ω and given by

$$G_\omega = \frac{\alpha}{v_t}\tilde{G}_k \quad \text{(D-14)}$$

α_∞ is given by;

$$\alpha_\infty = F_1\alpha_{\infty,1} + (1 - F_1)\alpha_{\infty,2} \quad \text{(D-15)}$$

where

$$\alpha_{\infty,1} = \frac{\beta_{i,1}}{\beta_\infty^*} - \frac{\kappa^2}{\sigma_{\omega,2}\sqrt{\beta_\infty^*}} \quad \text{(D-16)}$$

$$\alpha_{\infty,2} = \frac{\beta_{i,2}}{\beta_\infty^*} - \frac{\kappa^2}{\sigma_{\omega,2}\sqrt{\beta_\infty^*}} \quad \text{(D-17)}$$

Where κ is 0.41.

D.1.4 Modeling the Turbulence Dissipation

D.1.4.1 Dissipation of k

The term Y_k represents the dissipation of turbulence kinetic energy. $f_\beta *$ is a constant equal to 1. Thus

$$Y_k = \rho\beta^* k\omega \tag{D-18}$$

D.1.4.2 Dissipation of ω

The term Y_ω represents the dissipation of ω. f_β is a constant equal to 1.

$$Y_k = \rho\beta\omega^2 \tag{D-19}$$

Instead of having a constant value, β_i is given by

$$\beta_i = F_{i,1} + (1 - F_1)\beta_{i,2} \tag{D-20}$$

D.1.4.3 Model Constants

$\sigma_{k,1} = 1.176$, $\sigma_{\omega,1} = 2.0$, $\sigma_{k,2} = 1.0$, $\sigma_{\omega,2} = 1.168$, $\alpha_1 = 0.31$, $\beta_{i,1} = 0.075$, $\beta_{i,2} = 0.0828$

D.2 Reynolds Stress Model

D.2.1 Reynolds Stress Transport Equations

The exact transport equations for the transport of the Reynolds stresses, $\overline{u_j' u_j'}$, may be written as follows:

$$\frac{\partial}{\partial t}\left(\rho\overline{u_j'u_j'}\right)+\frac{\partial}{\partial x_k}\left(\rho u_k\overline{u_i'u_j'}\right)=$$

$$-\frac{\partial}{\partial x_k}\left[\rho\overline{u_i'u_j'u_k'}+\overline{p\left(\delta_{kj}u_i'+\delta_{ik}u_j'\right)}\right]+\frac{\partial}{\partial x_k}\left[\mu\frac{\partial}{\partial x_k}\left(\overline{u_i'u_j'}\right)\right]-\rho\left(\overline{u_i'u_k'}\frac{\partial u_j}{\partial x_k}+\overline{u_j'u_k'}\frac{\partial u_i}{\partial x_k}\right)-$$

$$\rho\beta\left(g_i\overline{u_j'\theta}+g_j\overline{u_i'\theta}\right)+\overline{\mathrm{p}\left(\frac{\partial u_i'}{\partial x_j}+\frac{\partial u_j'}{\partial x_i}\right)}-2\mu\,\overline{\frac{\partial u_i'}{\partial x_k}\frac{\partial u_j'}{\partial x_k}}-2\rho\Omega_{\mathrm{k}}\left(\overline{u_j'u_m'}\varepsilon_{\mathrm{ikm}}+\overline{u_i'u_m'}\varepsilon_{\mathrm{ikm}}\right)+$$

$$\mathrm{S_{user}} \qquad \text{(D-21)}$$

Of the various terms in these exact equations, C_{ij} , $D_{L,ij}$, P_{ij} , and F_{ij} do not require any modeling. However, D_T , G_{ij} , $\emptyset_{ij}$, and ε_{ij} need to be modeled to close the equations.

D.2.2 Modeling Turbulent Diffusive Transport

$D_{T,ij}$ can be modeled by the generalized gradient-diffusion model of Daly and Harlow:

$$D_{T,ij}=C_s\frac{\partial}{\partial x_k}\left(\rho\frac{k\overline{u_k'u_\ell'}}{\varepsilon}\frac{\partial\overline{u_i'u_j'}}{\partial x_\ell}\right) \qquad \text{(D-22)}$$

However, this equation can result in numerical instabilities, so it has been simplified in ANSYS FLUENT to use a scalar turbulent diffusivity as follows:

$$D_{T,ij}=\frac{\partial}{\partial x_k}\left(\rho\frac{\mu_t}{\sigma_k}\frac{\partial\overline{u_i'u_j'}}{\partial x_k}\right) \qquad \text{(D-23)}$$

Lien and Leschziner derived a value of $\sigma_k=0.82$ by applying the generalized gradient-diffusion model, to the case of a planar homogeneous shear flow. Note that $\sigma_k=1.0$.

D.2.3 Modeling the Pressure-Strain Term

D.2.3.1 Linear Pressure-Strain Model

By default in ANSYS FLUENT, the pressure-strain term, $\emptyset_{ij}$ is modeled according to the proposals by Gibson and Launder, Fu et al., and Launder.

The classical approach to modeling $\emptyset_{ij}$ uses the following decomposition:

$$\emptyset_{ij} = \emptyset_{ij,1} + \emptyset_{ij,2} + \emptyset_{ij,w} \quad \text{(D-24)}$$

Where, $\emptyset_{ij,1}$ is the slow pressure-strain term, also known as the return-to-isotropy term, $\emptyset_{ij,2}$ is called the rapid pressure-strain term, and $\emptyset_{ij,w}$ is the wall-reflection term.

The slow pressure-strain term,$\emptyset_{ij,1}$, is modeled as

$$\emptyset_{ij,1} \equiv -C_1 \rho \frac{\varepsilon}{k}\left[\overline{u_i' u_j'} - \frac{2}{3}\delta_{ij}k\right] \quad \text{(D-25)}$$

With C_1 = 1.8.

The rapid pressure-strain term,$\emptyset_{ij,2}$, is modeled as

$$\emptyset_{ij,2} \equiv -C_2\left[\left(P_{ij} + F_{ij} + 5/6G_{ij} - C_{ij}\right) - \frac{2}{3}\delta_{ij}(P + 5/6G - C)\right] \quad \text{(D-26)}$$

Where$C_2 = 0.60$, P_{ij} , F_{ij} , G_{ij} , and C_{ij} are defined as in (C-1)

$$P = \frac{1}{2}P_{kk}\,,\; G = \frac{1}{2}G_{kk}\,,\; C = \frac{1}{2}C_{kk} \quad \text{(D-27)}$$

The wall-reflection term, $\emptyset_{ij,w}$, is responsible for the redistribution of normal stresses near the wall. It tends to damp the normal stress perpendicular to the wall, while enhancing the stresses parallel to the wall. This term is modeled as

$$\emptyset_{ij,w} \equiv C_1' \frac{\varepsilon}{k}\left(\overline{u_k' u_m'} n_k n_m \delta_{ij} - \frac{2}{3}\overline{u_i' u_k'} n_j n_k - \frac{2}{3}\overline{u_j' u_k'} n_j n_k\right)\frac{C_\ell k^{2/3}}{\varepsilon d} + C_2'\left(\emptyset_{km,2} n_k n_m \delta_{ij} - \frac{3}{2}\emptyset_{ik,2} n_j n_k - \frac{3}{2}\emptyset_{jk,2} n_i n_k\right)\frac{C_\ell k^{3/2}}{\varepsilon d} \quad \text{(D-28)}$$

Where$C_1' = 0.5$, $C_2' = 0.3$, n_k is the x_k component of the unit normal to the wall, d is the normal distance to the wall, and $C_\ell = C_\mu^{3/4}/\kappa$ Where$C_\mu = 0.09$ and k is the von Kármán constant (= 0.4187)

$\emptyset_{ij,w}$ is included by default in the Reynolds stress model

D.2.3.2 Low-Re Modifications to the Linear Pressure-Strain Model

When the RSM is applied to near-wall flows using the enhanced wall treatment, the pressure-strain model needs to be modified. The modification used in ANSYS FLUENT specifies the values of C_1,C_2,$C_1^{'}$ and $C_2^{'}$ as functions of the Reynolds stress invariants and the turbulent Reynolds number, according to the suggestion of Launder and Shima:

$$C_1 = 1 + 2.58\mathrm{A}\mathrm{A}_2^{0.25}\{1 - \exp[-(0.0067\mathrm{Re}_\mathrm{t})^2]\} \quad \text{(D-29)}$$

$$C_2 = 0.75\sqrt{A} \quad \text{(D-30)}$$

$$C_1' = -\frac{2}{3}C_1 + 1.67 \quad \text{(D-31)}$$

$$C_2' = max\left[\frac{\frac{2}{3}C_2 - \frac{1}{6}}{C_2}, 0\right] \quad \text{(D-32)}$$

with the turbulent Reynolds number defined as $Re_t = (\rho k^2/\mu\varepsilon)$. The flatness parameter A and tensor invariants, A_2 andA_3, are defined as

$$A \equiv \left[1 - \frac{9}{8}(A_2 - A_3)\right] \quad \text{(D-33)}$$

$$A_2 = a_{ik}a_{ki} \quad \text{(D-34)}$$

$$A_3 = a_{ik}a_{kj}a_{ji} \quad \text{(D-35)}$$

a_{ij} is the Reynolds-stress anisotropy tensor, defined as

$$a_{ij} = -\left(\frac{-\rho\overline{u_i'u_j'} + \frac{2}{3}\rho k\delta_{ij}}{\rho k}\right) \quad \text{(D-36)}$$

The modifications detailed above are employed only when the enhanced wall treatment is selected in the Viscous Model Dialog Box.

D.2.4 Modeling the Turbulence Kinetic Energy

In general, when the turbulence kinetic energy is needed for modeling a specific term, it is obtained by taking the trace of the Reynolds stress tensor:

$$k = \frac{1}{2}\overline{u_i'u_i'} \quad \text{(D-37)}$$

An option is available in ANSYS FLUENT to solve a transport equation for the turbulence kinetic energy in order to obtain boundary conditions for the Reynolds stresses. In this case, the following model equation is used:

$$\frac{\partial}{\partial t}(\rho k) + \frac{\partial}{\partial x_i}(\rho k u_i) = \frac{\partial}{\partial x_j}\left[\left(\mu + \frac{\mu_t}{\sigma_k}\right)\frac{\partial k}{\partial x_j}\right] + \frac{1}{2}(P_{ii} + G_{ii}) - \rho\varepsilon(1 + 2M_t^2) + S_k \quad \text{(D-38)}$$

where$\sigma_k = 0.82$ and S_k is a user-defined source term.

Equation (D-38) is obtainable by contracting the modeled equation for the Reynolds stresses.

D.2.5 Modeling the Dissipation Rate

The dissipation tensor,ε_{ij}, is modeled as

$$\varepsilon_{ij} = \frac{2}{3}\delta_{ij}(\rho\varepsilon + Y_M) \tag{D-39}$$

Where $Y_M = 2\rho\varepsilon M_t^2$is an additional "dilatation dissipation" term according to the model by Sarkar. The turbulent Mach number in this term is defined as

$$M_t = \sqrt{\frac{k}{a^2}} \tag{D-40}$$

Where $a(\equiv \sqrt{\gamma RT})$,is the speed of sound. This compressibility modification always takes effect when the compressible form of the ideal gas law is used.

The scalar dissipation rate,ε , is computed with a model transport equation:

$$\frac{\partial}{\partial t}(\rho\varepsilon) + \frac{\partial}{\partial x_i}(\rho\varepsilon u_i) = \frac{\partial}{\partial x_j}\left[\left(\mu + \frac{\mu_t}{\sigma_\varepsilon}\right)\frac{\partial\varepsilon}{\partial x_j}\right] C_{\varepsilon 1}\frac{1}{2}[P_{ii} + C_{\varepsilon 3}G_{ii}]\frac{\varepsilon}{k} - C_{\varepsilon 2}\rho\frac{\varepsilon^2}{k} + S_\varepsilon \tag{D-41}$$

Where $\sigma_\varepsilon = 1.0$, $C_{\varepsilon 1} = 1.44$, $C_{\varepsilon 2} = 1.92$, $C_{\varepsilon 3}$ is evaluated as a function of the local flow direction relative to the gravitational vector and S_ε is a user-defined source term.

In the case when the Reynolds Stress model is coupled with the omega equation, the dissipation tensor ε_{ij} is modeled as

$$\varepsilon_{ij} = 2/3\,\delta_{ij}\rho\beta^*_{RMS}k\omega \tag{D-42}$$

D.2.6 Modeling the Turbulent Viscosity

The turbulent viscosity μ_t is computed similarly to the $k-\varepsilon$ models:

$$\mu_t = \rho C_\mu \frac{k^2}{\varepsilon} \tag{D-43}$$

Where $C_\mu = 0.09$.

Appendix E: ANSYS FLUENT Turbulence Models [35]

- Spalart-Allmaras model
- $k-\varepsilon$ models

  Standard $k-\varepsilon$ model

  Renormalization-group (RNG) $k-\varepsilon$ model

  Realizable $k-\varepsilon$ model

- $k-\omega$ models

  Standard $k-\omega$ model

  Shear-stress transport (SST) $k-\omega$ model

- v^2-f model (add-on)

  Transition $k-kl-\omega$ model

  Transition SST model

- Reynolds stress models (RSM)

  Linear pressure-strain RSM model

  Quadratic pressure-strain RSM model

  Low-Re stress-omega RSM model

- Scale-Adaptive Simulation (SAS) model

- Detached eddy simulation (DES) model, which includes one of the following RANS models.

Spalart-Allmaras$RANS$ model

Realizable $k-\varepsilon$ RANS model

$SST\ k-\omega$ RANS model

- Large eddy simulation (LES) model, which includes one of the following sub-scale models.

Smagorinsky-Lilly subgrid-scale model

WALE subgrid-scale model

Dynamic Smagorinsky model

Kinetic-energy transport subgrid-scale model